Article

SOURCE DATA | TRANSPARENT PROCESS | OPEN ACCESS

EMBO reports

BRD9 is a druggable component of interferon-stimulated gene expression and antiviral activity

Jacob Börold[1,2,†,‡], Davide Eletto[1,†], Idoia Busnadiego[1], Nina K Mair[1,2], Eva Moritz[1], Samira Schiefer[1,2], Nora Schmidt[1,§], Philipp P Petric[3,4], W Wei-Lynn Wong[5], Martin Schwemmle[3] & Benjamin G Hale[1,*]

Abstract

Interferon (IFN) induction of IFN-stimulated genes (ISGs) creates a formidable protective antiviral state. However, loss of appropriate control mechanisms can result in constitutive pathogenic ISG upregulation. Here, we used genome-scale loss-of-function screening to establish genes critical for IFN-induced transcription, identifying all expected members of the JAK-STAT signaling pathway and a previously unappreciated epigenetic reader, bromodomain-containing protein 9 (BRD9), the defining subunit of non-canonical BAF (ncBAF) chromatin-remodeling complexes. Genetic knockout or small-molecule-mediated degradation of BRD9 limits IFN-induced expression of a subset of ISGs in multiple cell types and prevents IFN from exerting full antiviral activity against several RNA and DNA viruses, including influenza virus, human immunodeficiency virus (HIV1), and herpes simplex virus (HSV1). Mechanistically, BRD9 acts at the level of transcription, and its IFN-triggered proximal association with the ISG transcriptional activator, STAT2, suggests a functional localization at selected ISG promoters. Furthermore, BRD9 relies on its intact acetyl-binding bromodomain and unique ncBAF scaffolding interaction with GLTSCR1/1L to promote IFN action. Given its druggability, BRD9 is an attractive target for dampening ISG expression under certain autoinflammatory conditions.

Keywords bromodomain; chromatin; epigenetics; interferon; virus
Subject Categories Chromatin, Transcription & Genomics; Immunology; Microbiology, Virology & Host Pathogen Interaction
DOI 10.15252/embr.202152823 | Received 9 March 2021 | Revised 23 July 2021 | Accepted 27 July 2021 | Published online 16 August 2021
EMBO Reports (2021) 22: e52823

Introduction

The type I interferon (IFN-α/β) system is a key component of the human innate immune response and acts as a first line of defense against invading pathogens such as viruses. At a general level, following host recognition of infection, secreted type I IFNs relay signals to target cells via their binding to cognate cell surface receptors (IFNAR1/IFNAR2) and the subsequent triggering of a well-defined phosphorylation-activation JAK-STAT signaling cascade involving the Janus kinases (JAK1/TYK2) and signal transducer and activator of transcription (STAT1/STAT2) proteins. Together with IFN-regulatory factor 9 (IRF9), activated STAT1 and STAT2 form a heterotrimeric transcription factor complex, termed ISGF3, that facilitates the transcription of hundreds of antiviral IFN-stimulated genes (ISGs) (Shaw *et al*, 2017; Lazear *et al*, 2019; Mesev *et al*, 2019). The critical nature of the IFN system in protecting humans against infection is exemplified by findings that some individuals with genetic defects in IFN pathway components can exhibit severe, or even fatal, viral diseases, particularly in the absence of pre-existing humoral immunity, as may be the case in young infants or following infection with an antigenically novel pandemic virus (Zhang *et al*, 2020; Duncan *et al*, 2021; Stertz & Hale, 2021).

It is essential that the IFN system is tightly regulated at the molecular level to prevent exuberant proinflammatory responses following infection (Ivashkiv & Donlin, 2014; Porritt & Hertzog, 2015; Lumb *et al*, 2017). Furthermore, uncontrolled activation of the IFN system caused by loss- or gain-of-function mutations in key regulators of the IFN pathway can be associated with aberrantly high levels of circulating IFNs and/or the constitutive expression of ISGs, leading to a broad range of autoinflammatory disorders known as interferonopathies (Zhang *et al*, 2015; Meuwissen *et al*, 2016; Rodero & Crow, 2016; Rodero *et al*, 2017; Duncan *et al*, 2019; Kong

1 Institute of Medical Virology, University of Zurich, Zurich, Switzerland
2 Life Science Zurich Graduate School, ETH and University of Zurich, Zurich, Switzerland
3 Faculty of Medicine, Institute of Virology, Freiburg University Medical Center, University of Freiburg, Freiburg, Germany
4 Spemann Graduate School of Biology and Medicine, University of Freiburg, Freiburg, Germany
5 Institute of Experimental Immunology, University of Zurich, Zurich, Switzerland
*Corresponding author. Tel: +41 44 634 2631; E-mail: hale.ben@virology.uzh.ch
†These authors contributed equally to this work
‡Present address: Department of Biosystems Science and Engineering, ETH Zurich, Basel, Switzerland
§Present address: Helmholtz Institute for RNA-based Infection Research, Helmholtz-Center for Infection Research, Wurzburg, Germany

et al, 2020; Martin-Fernandez *et al*, 2020; Rice *et al*, 2020). Proposed treatments for interferonopathies include JAK inhibitors (such as baricitinib (Sanchez *et al*, 2018), ruxolitinib (Alsohime *et al*, 2020), or tofacitinib (Alsohime *et al*, 2020)) to limit the signaling action of high levels of constitutively circulating IFN or inappropriate JAK-STAT regulation. However, while effective in treating interferonopathies, inhibiting critical components of the IFN signaling pathway can increase patient susceptibility to some viral infections (Kalunian, 2016; Marie *et al*, 2018). Therefore, a nuanced approach targeting factors involved in transcription of specific ISGs may be more appropriate (Marie *et al*, 2018).

In this study, we sought to leverage CRISPR/Cas9-mediated genome-scale loss-of-function screening to interrogate the IFN signaling cascade and identify human host factors required for ISG expression. Our screening results led us to focus on Bromodomain-containing protein 9 (BRD9), a defining subunit of specific chromatin-remodeling complexes (Alpsoy & Dykhuizen, 2018; Mashtalir *et al*, 2018), which has not previously been implicated in IFN responses. Many factors involved in transcriptional regulation via chromatin modification or remodeling play important roles in STAT-mediated ISG expression (Bhattacharya *et al*, 1996; Paulson *et al*, 1999; Huang *et al*, 2002; Liu *et al*, 2002; Paulson *et al*, 2002; Lau *et al*, 2003; Nusinzon & Horvath, 2003; Chang *et al*, 2004; Cui *et al*, 2004; Sakamoto *et al*, 2004; Gnatovskiy *et al*, 2013; Patel *et al*, 2013; Au-Yeung & Horvath, 2018; Marie *et al*, 2018; Lu *et al*, 2019), and some (such as histone deacetylases (HDACs) and bromodomain-containing proteins (Sakamoto *et al*, 2004; Patel *et al*, 2013; Au-Yeung & Horvath, 2018; Marie *et al*, 2018)) can be targeted pharmacologically. Here, we provide evidence that BRD9 contributes to the expression of a subset of ISGs (and thus the full antiviral action of IFN) via its unique functions in non-canonical BAF (BRG1- or BRM-associated factor; ncBAF) chromatin-remodeling complexes. Importantly, this contribution of BRD9 is conserved across numerous human cell types, including primary cells, and against multiple distinct viruses. Moreover, BRD9 can be specifically targeted for degradation by small-molecule compounds without impacting cell viability. Our data add insights into human factors required for the full activity of IFN and suggest a plausible therapeutic target to rationally temper detrimentally high ISG levels in some autoinflammatory disorders, including interferonopathies.

Results

A genome-scale loss-of-function screen identifies human genes important for interferon-stimulated gene expression

The type I IFN signaling pathway leading to induction of ISG expression is comprised of several canonical gene components, including receptors (*IFNAR1*, *IFNAR2*), kinases (*JAK1*, *TYK2*), and transcription factors (ISGF3: *STAT1*, *STAT2*, *IRF9*) (Fig 1A). To identify additional, previously uncharacterized, genes critical for the ability of IFN to signal and induce ISG expression, we performed a genome-scale FACS-based loss-of-function screen in the human lung epithelial cell line, A549. We used the GeCKOv2 CRISPR-Cas9 library, which contains a total of 123,411 CRISPR single-guide RNAs (sgRNAs) targeting 19,050 genes in the human genome with 6 guide RNAs per gene (Sanjana *et al*, 2014). First, we generated a sub-clone of an A549-based reporter cell line that expresses eGFP under control of an IFN-stimulated response element (A549/pr(ISRE).eGFP.A1) (Stewart *et al*, 2014) and confirmed that treatment of this sub-clone with IFN-α2 leads to high and homogenous expression of eGFP, with clear separation of IFN-stimulated and non-stimulated cell populations in flow cytometry analysis (Fig 1B). As a pre-screen validation, we next transduced this reporter cell line with all-in-one puromycin-resistant lentiviral vectors expressing Cas9 and several control sgRNAs selected from the GeCKOv2 human library. Following puromycin selection for 10 days to ensure protein depletion after CRISPR gene editing, we observed that a significant proportion of reporter cells transduced with sgRNAs targeting the canonical pathway components, *IFNAR1* or *STAT1*, failed to express eGFP in response to IFN-α2 stimulation (Fig 1C). As expected, reporter cells transduced with an sgRNA targeting a non-pathway component, *IFNLR1*, responded similarly to IFN-α2 stimulation as the parental cell line (Fig 1C). These data indicate that a FACS-based loss-of-function screen based on the GeCKOv2 human library can be used to identify components of the type I IFN signaling pathway in A549 cells.

We transduced A549/pr(ISRE).eGFP.A1 cells with a pool of all-in-one puromycin-resistant lentiviral vectors (lentiCRISPRv2) comprising the entire GeCKOv2 human library at a multiplicity of infection (MOI) of 0.3 focus forming units (FFU)/cell to ensure that most transduced cells received only one sgRNA. We then selected the cells with puromycin for 10 days to ensure that only transduced cells survived and to allow for protein depletion after genome editing. Puromycin-selected reporter cells were then treated (or not) with 1,000 IU/ml IFN-α2 for 16 h to stimulate eGFP expression, and FACS was used to enrich for eGFP-negative cells that failed to respond to IFN-α2 (Fig 1D). Following extraction of genomic DNA from both the parental library-transduced reporter cell line and the eGFP-negative cells that failed to respond to IFN treatment, sgRNA abundance was determined via targeted sequencing (Fig 1D). Two biological replicates of the screen were performed, and for each replicate, the adjusted robust-rank aggregation (αRRA) feature of the PinAPL-Py platform was used to determine gene-level rankings (based on relative enrichment of each individual sgRNA (Kolde *et al*, 2012; Spahn *et al*, 2017)) for loss-of-function events leading to IFN non-responsiveness. From this genome-scale screen, we identified 8 genes that exhibited significant αRRA enrichment ($P < 0.01$) in both biological replicates (Fig 1E, Dataset EV1). The robustness of our results was validated by the observation that 7 of these 8 genes comprise all the known essential factors in the canonical type I IFN signaling pathway leading to ISG expression: *IFNAR1*, *IFNAR2*, *JAK1*, *TYK2*, *STAT1*, *STAT2*, and *IRF9*. The 8th gene found to be significantly enriched in both our screens was *BRD9*, which has not previously been characterized for its role in the type I IFN signaling pathway. To validate this result, we performed independent experiments using individually cloned and arrayed sgRNAs and could confirm that all 6 *BRD9*-targeting sgRNAs within the GeCKOv2 human library limit IFN-α2-stimulated expression of eGFP in A549/pr(ISRE).eGFP.A1 cells (Fig EV1A). Notably, a recent independent genome-wide screening approach using insertional mutagenesis in HAP1 cells also identified *BRD9* enrichment when searching for positive regulators of type III IFN-stimulated gene expression (Lumb *et al*, 2017), which is thought to use the same intracellular signaling machinery as type I IFN (Lazear *et al*, 2019). Thus, our genome-

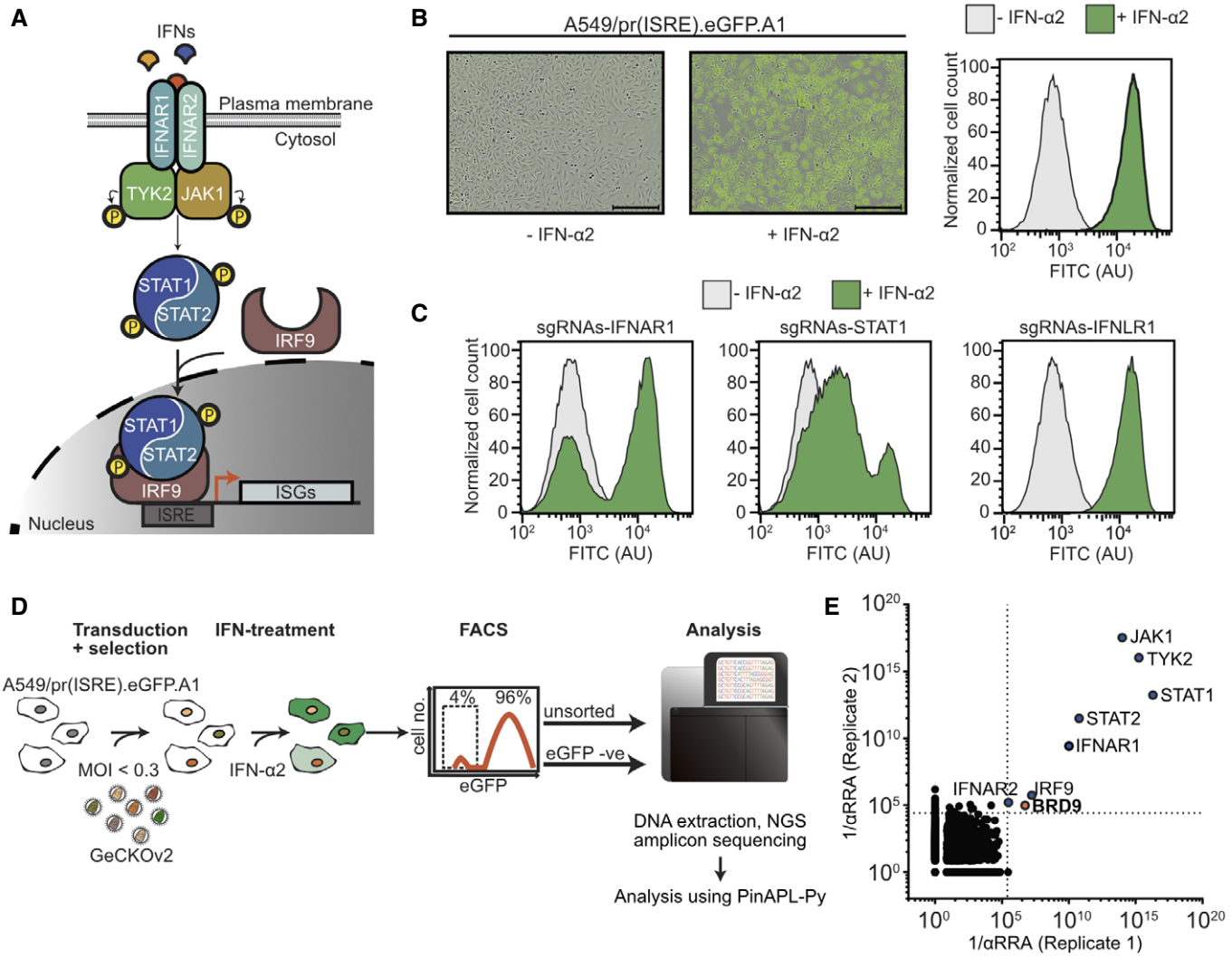

Figure 1. A genome-scale loss-of-function screen identifies human genes important for interferon-stimulated gene expression.

A Schematic representation of the type I IFN signaling pathway in human cells.

B Stimulation of A549/pr(ISRE).eGFP.A1 cells with 1,000 IU/ml of IFN-α2 for 16 h results in high and homogeneous expression of eGFP as determined by fluorescence microscopy (left panels, scale bars indicate 300 μm) and flow cytometry (right panel). The FITC channel was used to monitor eGFP levels by flow cytometry, and AU refers to arbitrary units. Data are representative of at least two biological replicates.

C A549/pr(ISRE).eGFP.A1 cells were transduced for at least 10 days with lentivirus pools expressing Cas9 and sgRNAs targeting the indicated host genes. eGFP levels following 16 h of IFN-α2 treatment (1,000 IU/ml) or mock were determined by flow cytometry. Data are representative of at least two biological replicates.

D Workflow overview of the genome-scale loss-of-function screen for essential IFN signaling components using the full GeCKOv2 CRISPR-Cas9 library.

E 1/αRRA scores from two biological replicates of the genome-scale screen. Dotted lines represent the significance cutoffs for each replicate. Genes identified as significant in both screens are highlighted.

Data information: See also Fig EV1 and Dataset EV1.

scale loss-of-function screen successfully identified both known genetic components of the human type I IFN signaling pathway and a new uncharacterized factor, *BRD9*.

BRD9 is important for interferon-stimulated gene transcription and antiviral activity

BRD9 encodes Bromodomain-containing protein 9 (BRD9). BRD9 is a defining subunit of the recently described non-canonical BAF (ncBAF) complex, one of three major distinct types of ATP-dependent chromatin-remodeling complexes (together with canonical BAF and the polybromo-associated, PBAF) that govern DNA accessibility and thus appropriate regulation of gene transcriptional programs (Fig EV1B) (Alpsoy & Dykhuizen, 2018; Mashtalir *et al*, 2018). To initially understand the specificity of our CRISPR screen finding, we used siRNA pools to deplete unique components of either ncBAF (BRD9 and GLTSCR1) or PBAF (BRD7 and ARID2) and study the contribution of these BAF complexes to the antiviral action of human type I IFN. Notably, treatment of A549 cells with siRNAs that target BRD9 or GLTSCR1, but not BRD7 or ARID2, led

to a reproducible (although not statistically significant) reduction in the ability of IFN-α2 to fully protect cells from infection with the IFN-sensitive vesicular stomatitis virus (VSV) (Fig EV1C). The relatively small, yet highly consistent, functional effects observed may be due to inefficient depletion of the respective factors by the siRNAs used, which were not assessed in this secondary screening assay. Nevertheless, these data independently support the evidence from the genome-scale CRISPR screen that BRD9 contributes to IFN function and additionally indicate that the ncBAF complex may have a specific role in this pathway.

To dissect further the functions of BRD9 in IFN signaling and to solidify the siRNA-based findings, we used CRISPR/Cas9 to generate two independent sets of A549-based BRD9 knockout (KO) and control (CTRL) clonal cell lines (termed CTRL#1, CTRL#2, BRD9-KO#1, and BRD9-KO#2). Amplicon sequencing of genomic DNA confirmed the KO and CTRL genotypes of all clones, and Western blot validated the complete loss of BRD9 protein expression in both KO clones (Figs 2A and B, EV2A and B). Loss of BRD9 did not interfere with IFN-α2-induced phosphorylation of JAK1 or STAT1, or with the IFN-α2-induced translocation of phosphorylated STAT1 to the nucleus (Fig 2C and D). However, consistent with its known role in regulation of chromatin remodeling and gene transcription, loss of BRD9 led to a reduction in IFN-α2-induced *MX1* mRNA levels and a consequent reduction in IFN-α2-induced MxA protein levels (Figs 2E and F, and EV2C). The effect of BRD9 on inducible gene expression was specific to IFN-α2 stimulation, as TNF-α-induced *NFKBIA* mRNA levels were unaffected by loss of BRD9 (Fig EV2G). Importantly, loss of BRD9 rendered cells unable to mount a fully effective IFN-α2-stimulated antiviral response against influenza A virus (IAV) (Figs 2G and EV2D). To confirm that the observed phenotypes were due only to the loss of BRD9 (and not to off-target CRISPR edits), we used a lentivirus vector to reconstitute BRD9 expression. Reconstitution of BRD9 in BRD9-KO cells restored the ability of IFN-α2 to induce MxA protein levels (Figs 2H and EV2E) and promoted the ability of IFN-α2 to mediate antiviral activity against IAV (Figs 2I and EV2F). These results identify a role for BRD9 in type I IFN signaling at the level of ISG transcription and reveal that this role is critical for the effective antiviral activity of IFN.

Targeted degradation of BRD9 reveals its cell type-independent contribution to interferon-stimulated antiviral activity against multiple viruses

We used a targeted chemical degrader of BRD9, dBRD9-A, as a tool to efficiently deplete cells of BRD9 protein in the absence of genetic manipulation. dBRD9-A is a highly optimized heterobifunctional ligand that specifically targets the BRD9 bromodomain and bridges it to the Cereblon E3 ubiquitin ligase complex, thereby targeting BRD9 protein for proteasome-mediated degradation (Remillard *et al*, 2017; Brien *et al*, 2018) (Fig 3A). Treatment of A549 cells with 125 nM dBRD9-A led to a rapid depletion of BRD9 protein within 6 h (Fig 3B), and we could confirm the high specificity of this depletion as levels of the closely related BRD7 protein were unaffected (Fig 3C). Importantly, and consistent with our ability to generate BRD9-KO A549 cells, BRD9 degradation by dBRD9-A treatment had negligible effects on cell viability (Fig EV3A). Using dBRD9-A, we confirmed that BRD9 depletion leads to a reduction in IFN-α2-induced MxA protein levels in A549 cells (Fig 3D) and to an ineffective mounting of IFN-α2-stimulated antiviral responses against IAV (Fig 3E). Such defective mounting of antiviral responses was not limited to the inefficient control of IAV, as dBRD9-A-treated A549 cells also failed to induce full IFN-α2-mediated antiviral programs against another RNA virus (VSV), a DNA virus (herpes simplex virus type 1, HSV1), and a retrovirus (human immunodeficiency virus type 1, HIV1) (Fig 3F–H). In these assays, no effects of dBRD9-A treatment on virus replication were noted in the absence of IFN-α2 treatment. In addition, dBRD9-A treatment of a panel of human cell lines (including Hep2, Huh-7, Calu-3, and U87MG), murine 3T3, primary-like human MRC-5, and primary undifferentiated human tracheobronchial epithelial (HTBE) cells revealed that BRD9 contributes to IFN-stimulated antiviral activity in a broad range of cell types and hosts (Figs 3I and L, and EV3B–D). The independent ability of dBRD9-A to recapitulate the results from BRD9-KO cells supports the hypothesis that BRD9 promotes IFN-stimulated gene expression. Furthermore, these data highlight the cell type-independent function of BRD9 in the IFN-mediated antiviral response against different viruses.

BRD9 promotes the interferon-stimulated expression of a subset of antiviral genes

To gain a deeper, and system-wide understanding of the spectrum of IFN-stimulated genes regulated by BRD9, we conducted a transcriptomic experiment to identify genes differentially expressed upon IFN-α2 stimulation of A549 cells in the presence or absence of dBRD9-A (Fig 4A). Experiments were performed three independent times, and we defined up- or downregulated genes using cutoff values of 2-fold-change (FC) and a *P*-value of ≤ 0.001. Using these criteria, we identified 333 significantly upregulated, and 5 significantly downregulated, gene transcripts in A549 cells following 6 h of 100 IU/ml IFN-α2 treatment (Fig 4B, Dataset EV2). Notably, dBRD9-A treatment in the absence of IFN-α2 resulted in the downregulation of only 11 gene transcripts, and none of these genes have previously been implicated in the type I IFN signaling pathway (top 5 downregulated: *PCED1B*, *NAMPT*, *CLDN2*, *NNMT*, and *ARPIN*) (Dataset EV2). However, we note that at least 3 of these dBRD9-A-regulated genes (*PCED1B*, *NAMPT*, and *NNMT*) are putative mammalian ISGs (Shaw *et al*, 2017) and may therefore be basally regulated by STAT transcription factor complexes. Of the 333 IFN-upregulated genes (ISGs) we identified in A549 cells, we found that prior dBRD9-A treatment led to significantly reduced induction of 29 ISGs, including many ISGs known to harbor antiviral activity against the viruses used in this study, such as *MX1*, *MX2*, *IFITM1*, *IFITM3*, *IDO1*, and *BST2* (Fig 4C, Dataset EV2). Importantly, the expression of many ISGs was not affected by dBRD9-A treatment, and it was notable that the impact of dBRD9-A on ISG expression did not appear to directly correlate (positively or negatively) with gene induction levels by IFN-α2, indicating gene specificity (Fig 4D and E). Targeted RT–qPCR analysis confirmed the inhibitory effect of dBRD9-A treatment on IFN-α2-stimulated expression of *MX1*, *MX2*, and *IFITM1*, but not *IFIT1* or *ISG15* (Fig 4F). Strikingly, this gene-specific pattern was not identical between different human cell lines (Fig EV4A–C), suggesting that epigenetic factors regulating chromatin state (rather than specific ISG promoter sequences) likely determine the contribution of BRD9 to ISG expression. Indeed, we

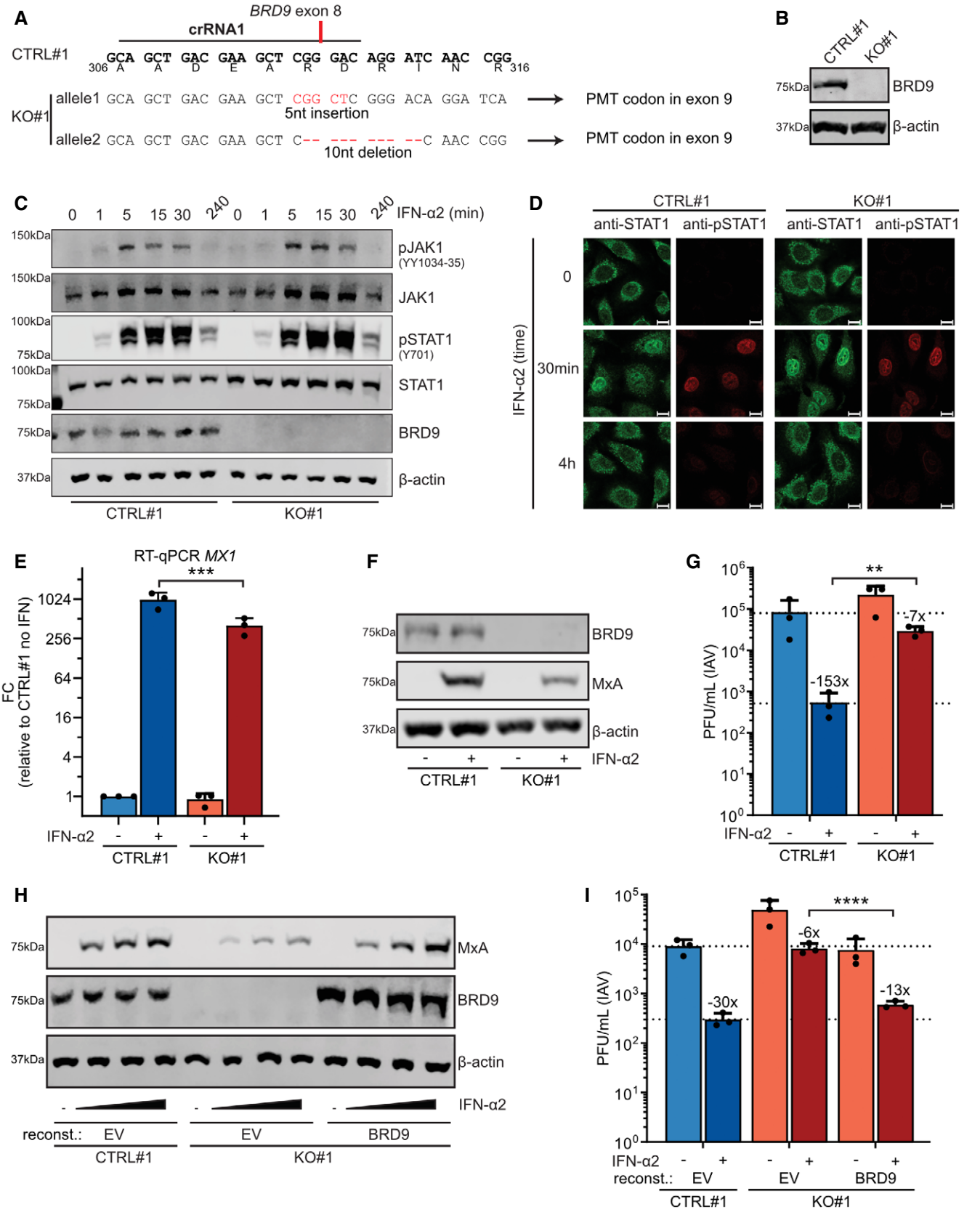
A
BRD9 exon 8
crRNA1
CTRL#1
306 GCA GCT GAC GAA GCT CGG GAC AGG ATC AAC CGG 316
A A D E A R D R I N R
KO#1
allele1 GCA GCT GAC GAA GCT CGG CTC GGG ACA GGA TCA
5nt insertion
PMT codon in exon 9
allele2 GCA GCT GAC GAA GCT C-- --- --- --C AAC CGG
10nt deletion
PMT codon in exon 9
B
CTRL#1
KO#1
75kDa
BRD9
37kDa
β-actin
C
0 1 5 15 30 240 0 1 5 15 30 240 IFN-α2 (min)
150kDa
pJAK1
(YY1034-35)
150kDa
JAK1
100kDa
75kDa
pSTAT1
(Y701)
100kDa
75kDa
STAT1
75kDa
BRD9
37kDa
β-actin
CTRL#1
KO#1
D
CTRL#1
KO#1
anti-STAT1
anti-pSTAT1
anti-STAT1
anti-pSTAT1
IFN-α2 (time)
0
30min
4h
E
RT-qPCR MX1
***
FC
(relative to CTRL#1 no IFN)
1024
256
64
16
4
1
IFN-α2 - + - +
CTRL#1
KO#1
F
75kDa
BRD9
75kDa
MxA
37kDa
β-actin
- + - + IFN-α2
CTRL#1
KO#1
G
PFU/mL (IAV)
**
-153x
-7x
IFN-α2 - + - +
CTRL#1
KO#1
H
75kDa
MxA
75kDa
BRD9
37kDa
β-actin
IFN-α2
reconst.: EV EV BRD9
CTRL#1
KO#1
I
PFU/mL (IAV)
****
-30x
-6x
-13x
IFN-α2 - + - + - +
reconst.: EV EV BRD9
CTRL#1
KO#1

Figure 2.

Figure 2. BRD9 is important for interferon-stimulated gene transcription and antiviral activity.

A An A549-derived BRD9-KO cell clone (KO#1) was generated using a crRNA targeting exon 8 of *BRD9*. The target sequence of the crRNA (termed crRNA1), and the resulting genomic alterations determined by NGS for the two *BRD9* alleles, is shown in comparison to an unedited control clone (CTRL#1). Generated indels lead to a premature termination codon (PMT) in the following exon. Encoded amino acids are shown below the CTRL nucleotide sequence.

B Western blot analysis of lysates from CTRL#1 or BRD9-KO#1 cells. BRD9 and β-actin were detected with specific antibodies. Data are representative of at least two biological replicates.

C Western blot analysis of CTRL#1 or BRD9-KO#1 lysates from cells treated for the indicated times with 1,000 IU/ml of IFN-α2. The indicated proteins were detected with specific antibodies. Data are representative of at least two biological replicates.

D Immunofluorescence analysis of CTRL#1 or BRD9-KO#1 cells treated for the indicated times with 1,000 IU/ml of IFN-α2. The indicated proteins were detected with specific antibodies. Data are representative of at least two biological replicates. Scale bars indicate 10 μm.

E RT–qPCR analysis of *MX1* levels in CTRL#1 or BRD9-KO#1 cells following treatment, or not, with 100 IU/mL of IFN-α2 for 6 h. *GAPDH* transcript levels were used for normalization. Data represent means and standard deviations of fold expression changes (relative to CTRL#1 without IFN-α2 treatment) from $n = 3$ biological replicates (individual data points shown). Statistical significance was determined by unpaired 2-tailed *t*-test on ΔC_t values (***$P < 0.001$).

F Western blot analysis of CTRL#1 or BRD9-KO#1 lysates from cells treated or not for 16 h with 1,000 IU/ml of IFN-α2. The indicated proteins were detected with specific antibodies. Data are representative of at least two biological replicates.

G CTRL#1 or BRD9-KO#1 cells were treated, or not, with 1,000 IU/ml of IFN-α2 for 16 h prior to infection with IAV (WSN/33) at an MOI of 0.01 PFU/cell. Viral titers were determined after 24 h by plaque assay.

H CTRL#1 or BRD9-KO#1 cells were stably transduced with BRD9-expressing, or control (EV, empty vector), lentiviruses and treated with a range of IFN-α2 concentrations (0, 10, 100, 1,000 IU/ml) for 16 h prior to lysis and analysis for the indicated proteins by Western blot. Data are representative of at least two biological replicates.

I CTRL#1 or BRD9-KO#1 cells were stably transduced with BRD9-expressing, or control (EV, empty vector), lentiviruses and treated with 1,000 IU/ml of IFN-α2 for 16 h prior to infection with IAV (WSN/33) at an MOI of 0.01 PFU/cell. Viral titers were determined after 24 h by plaque assay.

Data information: For (G) and (I), data represent means and standard deviations from $n = 3$ biological experiments (individual data points shown). Statistical significance was determined by 1-way ANOVA on log-transformed plaque counts (**$P < 0.001$; ****$P < 0.0001$). Dotted lines are a visual guide for maximum and minimum virus replication in control cells in the absence and presence of IFN-α2, respectively. Numbers above IFN-α2-treated bars indicate their approximate difference to the respective untreated conditions. See also Fig EV2.
Source data are available online for this figure.

could not find an enrichment of any specific promoter sequences in the ISGs regulated by dBRD9-A treatment. These data indicate that BRD9 has a role in promoting the IFN-stimulated expression of a broad set of specific ISGs and that this set of ISGs may be cell type, or cell state, specific.

BRD9 function requires its acetyl-binding activity and unique DUF3512 scaffolding domain

BRD9 comprises an N-terminal bromodomain and a C-terminal DUF3512 scaffolding domain that mediates a specific interaction with the GLTSCR1/1L component of ncBAF (Mashtalir *et al*, 2018; Wang *et al*, 2019) (Fig 5A). Bromodomains are reader modules of acylated residues and generally mediate the interaction of protein complexes, such as ncBAF, with DNA via acetylated histones. The bromodomain of BRD9 is reported to exhibit high binding affinity toward acetylated lysines as well as an unconventional binding of butyrylated lysines (Flynn *et al*, 2015). To test the impact of BRD9 activities on type I IFN-induced function, we initially constructed a series of BRD9 mutants that either lacked the entire bromodomain (dBD), or which contained single amino acid substitutions known to abolish the ability of BRD9 to bind acetylated lysines (N216A) or

Figure 3. Targeted degradation of BRD9 reveals its cell type-independent contribution to interferon-stimulated antiviral activity against multiple viruses.

A Schematic representation of the mechanism of action of dBRD9-A. dBRD9-A simultaneously recruits the ubiquitin E3 ligase Cereblon (CRBN) to the bromodomain (BD) of BRD9, thereby facilitating the ubiquitination and degradation of BRD9.

B A549 cells were treated for the indicated time with either DMSO or 125 nM dBRD9-A. Following lysis and Western blot analysis for the indicated proteins, BRD9 levels were quantified by densitometry and made relative to levels in DMSO-treated cells (% below). Data are representative of at least two biological replicates.

C A549 cells were treated with 125 nM dBRD9-A (+) or DMSO (–) for 6 h prior to lysis and analysis by Western blot for the indicated proteins. Data are representative of at least two biological replicates.

D A549 cells were treated with 125 nM dBRD9-A (+) or DMSO (–) for 6 h prior stimulation with 1,000 IU/ml of IFN-α2 for 16 h. Following lysis, Western blot was used to detect levels of the indicated proteins. Data are representative of at least two biological replicates.

E A549 cells were treated as described in (D), but following stimulation with 1,000 IU/ml of IFN-α2 for 16 h were infected with IAV (WSN/33) at an MOI of 0.01 PFU/cell. Viral titers were determined after 24 h by plaque assay. Data represent means and standard deviations from $n = 3$ biological experiments (individual data points shown). Statistical significance was determined by 1-way ANOVA on log-transformed plaque counts (***$P < 0.001$).

F–H A549 cells were treated as described in (E), but IFN-α2 concentrations ranged from 10 to 1,000 IU/ml depending upon the virus, and infections were similarly performed but with: VSV-GFP (F); HSV1-GFP (G); or VSV-G pseudotyped HIV1-GFP (H).

I–L Hep2 (I), Huh-7 (J), MRC-5 (K), and undifferentiated HTBE (L) were treated and infected with VSV-GFP as in (F).

Data information: For F-L, total integrated green fluorescent intensities were determined using the Incucyte live-cell analysis system after 10 h (G), 24 h (F, I-L), or 48 h (H). Data represent means and standard deviations from $n = 3$ biological experiments (individual data points shown). Statistical significance was determined by 1-way ANOVA on log-transformed intensity values (*$P < 0.05$; **$P < 0.01$; ***$P < 0.001$; ****$P < 0.0001$). For E-L, dotted lines are a visual guide for maximum and minimum virus replication in control cells in the absence and presence of IFN-α2, respectively. Numbers above IFN-α2-treated bars indicate their approximate difference to the respective untreated conditions. See also Fig EV3.
Source data are available online for this figure.

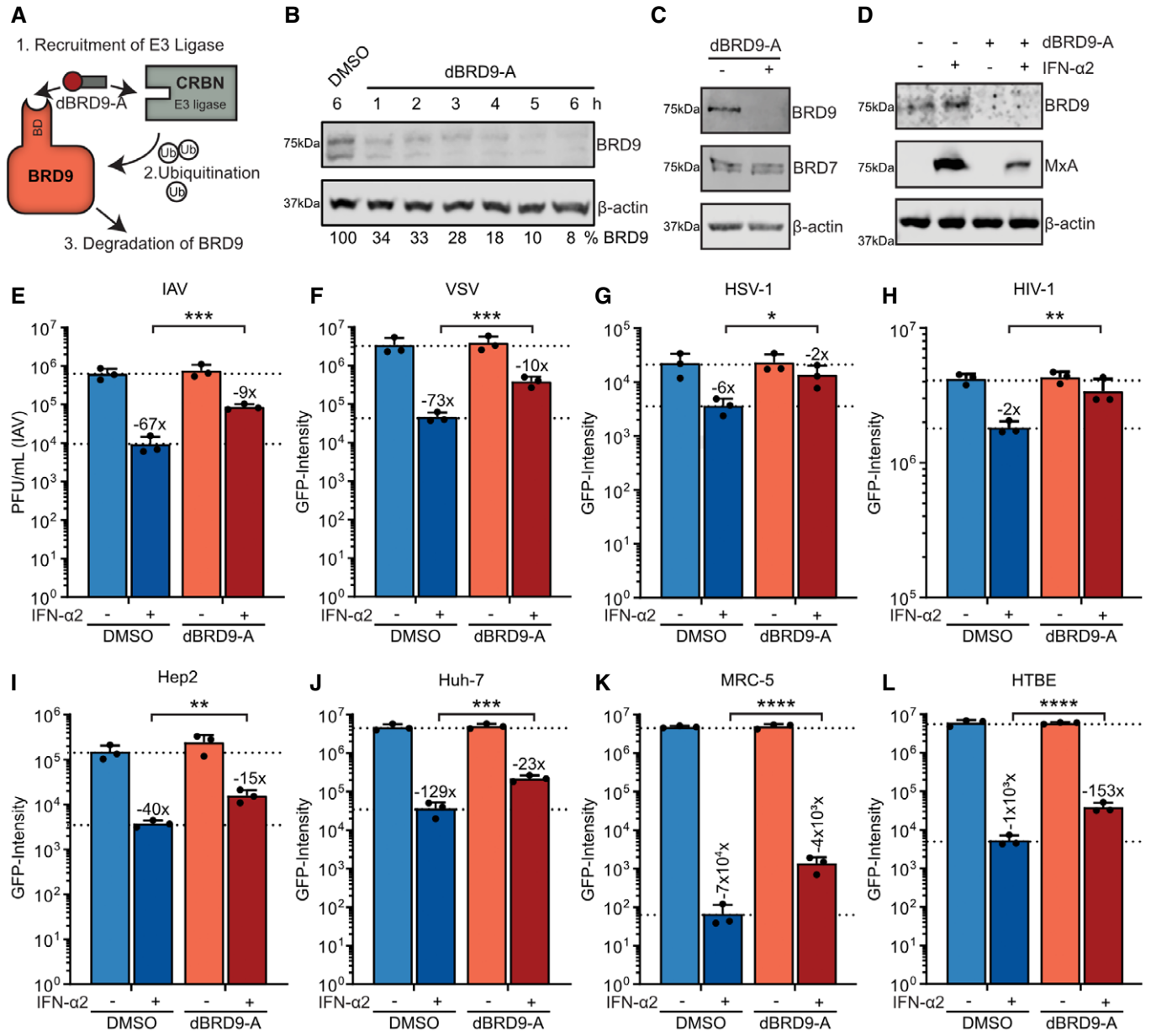

Figure 3.

butyrylated lysines (M208I) (Flynn *et al*, 2015). Furthermore, we used CRISPR/Cas9 to generate an independent set of A549-based BRD9 knockout (KO) and control (CTRL) clonal cell lines (termed CTRL#3 and BRD9-KO#3) that were both derived from a highly IFN-sensitive A549 sub-clone, 2D8, that is regularly used in our laboratory. The rationale for making this additional CTRL/KO pair on a more homogenous genetic background was to increase the dynamic range of antiviral assays and thereby improve the study of BRD9 mutants. Amplicon sequencing of genomic DNA confirmed the KO and CTRL genotypes of these clones, and Western blot validated the loss of BRD9 protein expression in the KO#3 clone (Fig EV5A and B). Lentivirus-mediated reconstitution of BRD9-KO#3 cells with either wild-type (wt) BRD9 or the individual BRD9 mutants revealed that all constructs were expressed similarly (Fig 5A). However, there were clear differences in the ability of each BRD9 construct to restore the antiviral activity of IFN-α2: as compared to wt BRD9, BRD9 mutants lacking the entire bromodomain (dBD) or lacking acetyl-lysine binding (N216A) were inefficient at reconstituting IFN-α2 activity, while the BRD9 mutant lacking butyryl-lysine binding (M208I) functioned similarly to wt BRD9 (Fig 5B). These data suggest that acetyl (but not butyryl) binding by the BRD9 bromodomain is important, although apparently not essential, for the function of BRD9 in the context of a type I IFN-mediated antiviral response.

We next investigated the contribution of the BRD9 DUF3512 domain to type I IFN-mediated antiviral activity. Highly homologous DUF3512 domains are shared between BRD9 and the closely related BRD7, although each serves as a specific scaffolding interaction

platform for either the ncBAF component, GLTSCR1/1L, or the PBAF component, ARID2, respectively (Mashtalir *et al*, 2018; Wang *et al*, 2019) (Fig EV1B). We generated N-terminally HA-tagged chimeras between BRD9 and BRD7 (Fig 5C–E), as well as specific BRD7/BRD9 domain swap constructs (Fig 5F–I) (Michel *et al*, 2018), and used lentivirus vectors to reconstitute BRD9-KO#3 cells with each variant. All constructs were expressed similarly to their respective wt BRD9 control and at levels above endogenous BRD9 levels in unedited CTRL#3 cells (Fig 5D and G). Furthermore, we confirmed that wt BRD9 could specifically co-precipitate GLTSCR1, and not ARID2, but that such interactions could be reversed by replacing the DUF3512 domain of BRD9 with that of BRD7 (Fig 5H). As compared to wt BRD9, BRD7 expression was unable to restore the antiviral activity of IFN-α2 in BRD9-KO#3 cells (Fig 5E), a result consistent with our

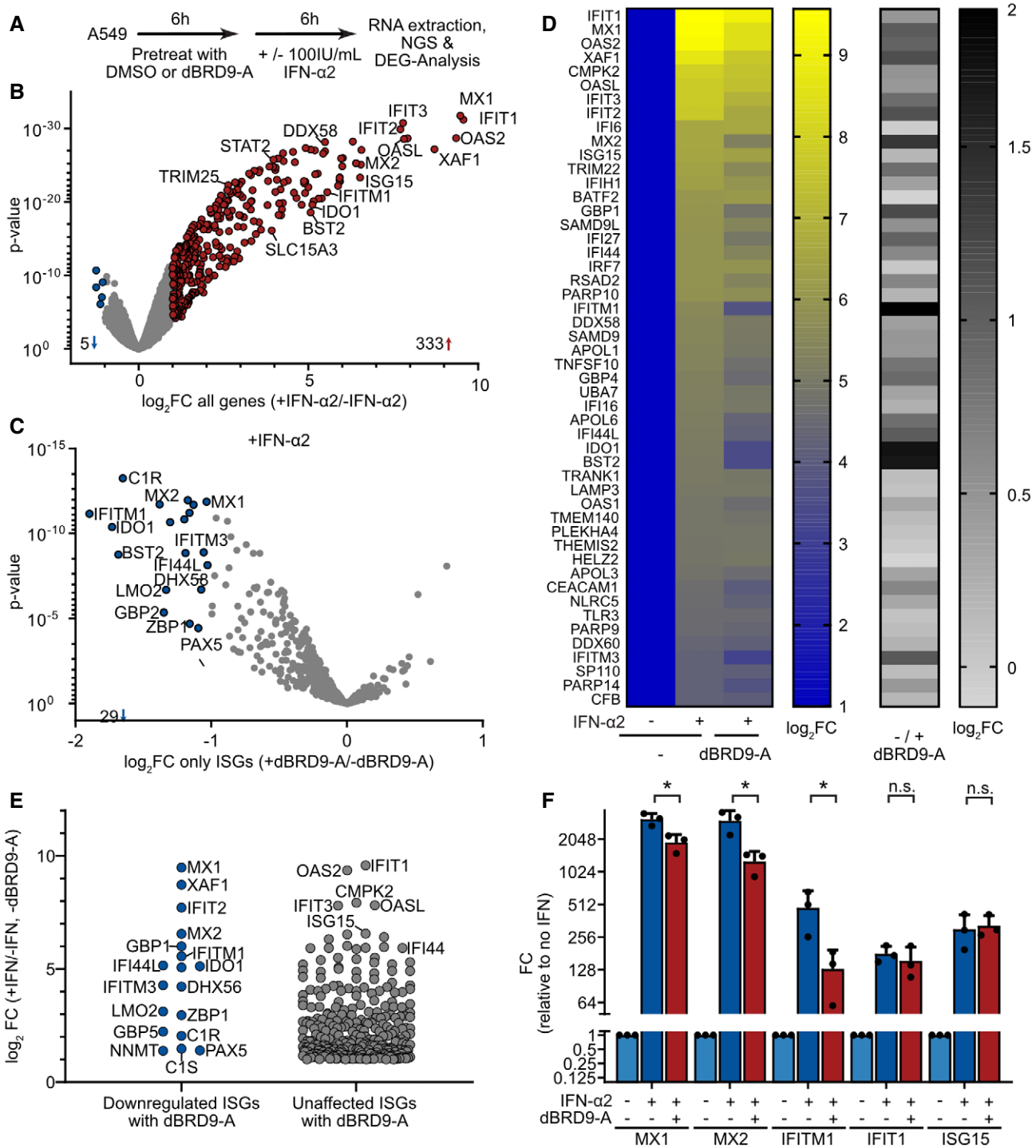

Figure 4.

Figure 4. BRD9 promotes the interferon-stimulated expression of a subset of antiviral genes.

A Overview of the dBRD9-A transcriptomics experiment in A549 cells.

B Up-regulated (red) and downregulated (blue) genes identified in A549 cells following treatment with 100 IU/ml IFN-α2 for 6 h: ISGs were defined as induced by IFN-α2 with FC > 2, *P*-value ≤ 0.001.

C Impact of dBRD9-A pretreatment on the induction of ISGs identified in (B). Colors indicate IFN-induced transcripts significantly affected (blue) or unaffected (gray) by dBRD9-A pretreatment (FC > 2, *P*-value ≤ 0.001).

D Heatmaps highlighting the gene expression changes observed with each treatment. Left: the top 50 ISGs, ranked by IFN-induced expression (B), were compared with respect to the impact that dBRD9-A pretreatment had on induction. Right: comparative fold change in induction for each ISG in the presence or absence of dBRD9-A.

E ISG expression level following IFN-α2 stimulation, grouped by whether they were affected or not by dBRD9-A pretreatment (see C).

F RT–qPCR confirmation of transcriptomics results for selected transcripts (*MX1*, *MX2*, *IFITM1*, *ISG15*, and *IFIT1*) in A549 cells treated as outlined in (A). *GAPDH* transcript levels were used for normalization. Data represent means and standard deviations from $n = 3$ biological experiments (individual data points shown). Statistical significance was determined by unpaired 2-tailed *t*-test on ΔC_t values (*$P < 0.05$; n.s. not significant).

Data information: See also Fig EV4.

previous siRNA-based observations (Fig EV1C) which again highlights the specificity of BRD9/ncBAF function in this pathway. Notably, constructs consisting of the BRD9 bromodomain in the context of the BRD7 DUF3512 domain also failed to restore the antiviral activity of IFN-α2 in BRD9-KO#3 cells, while constructs containing the BRD9 DUF3512 domain (even in the context of the BRD7 bromodomain) exhibited a strong ability to restore IFN-α2 function, albeit not to levels equivalent to full-length BRD9 (Figs 5E and I). These data suggest that acetyl-binding is important for BRD9 function in the type I IFN-mediated antiviral response somewhat independently of bromodomain identity. Furthermore, in this antiviral process, BRD9 must act via the specific ncBAF complex, likely using GLTSCR1/1L, as altering the DUF3512-mediated complex composition attenuated BRD9 function in the type I IFN-mediated antiviral response. Such features of general BRD9 function have been observed previously (Hohmann *et al*, 2016), and it is noteworthy that *GLTSCR1* was enriched in a previous screen to identify positive regulators of type III IFN-stimulated gene expression (Lumb *et al*, 2017), which is consistent with our own siRNA-based observations (Fig EV1C). These data support the hypothesis of specific involvement of the ncBAF complex in promoting IFN-stimulated gene expression and antiviral activity.

Interferon induces the close proximity of BRD9 with STAT2

To further understand the involvement of BRD9 (and the ncBAF complex) in IFN-stimulated gene expression, we sought to identify the BRD9 protein interactome in A549 cells, as well as any IFN-induced changes to this interactome. We therefore N-terminally tagged wt BRD9 with the highly active and promiscuous biotin ligase, TurboID (Branon *et al*, 2018), with the aim of biotinylating proteins proximal to BRD9 in living cells and subsequently capturing them with streptavidin beads prior to identification by mass spectrometry. The benefits of using TurboID for detecting protein–protein interactions include the *in situ* nature of biotin labeling reducing the likelihood of identifying artefactual interactions, and the ability to identify weak or transient interactions in the local environment that might otherwise be lost with other affinity-based methods (Branon *et al*, 2018). For these assays, TurboID-tagged mCherry served as a negative control (Fig 6A). Using lentivirus vectors, both TurboID-tagged mCherry and TurboID-tagged BRD9 were independently expressed in A549 cells, and their biotinylated interactomes under resting conditions were determined (Fig 6B). By comparison with the mCherry-negative control across 3 biological replicates, we identified (with high confidence) 145 proteins in close proximity to BRD9 under these non-stimulated conditions (Dataset EV3). Notable among the interactors were 7 subunits of the ncBAF complex, including GLTSCR1/1L (also known as BICRA/L) (Fig 6C). Furthermore, ARID2, a specific interactor of the BRD7 DUF3512 domain and key component of the PBAF complex, was not identified as a BRD9 interactor. These findings are fully in line with our own confirmatory co-immunoprecipitation data presented in Fig 5H. Gene ontology (GO) analysis also revealed that these 145 protein interactors are functionally enriched for cellular processes including chromatin remodeling/modification, regulation of transcription, and nucleosome/histone activity (Fig 6D). These analyses validate the specificity of our approach in identifying proteins in close proximity to BRD9 and the ncBAF complex in A549 cells.

We next used the TurboID assay to study the BRD9 interactome in the presence or absence of a 60-min stimulation with IFN-α2 (Fig 6B), which was chosen as a time point representing the initiation of ISG transcription. The deduced BRD9 interactomes under these two conditions were essentially identical, suggesting that the pre-formed BRD9-nucleated ncBAF complex is not perturbed. However, IFN-α2 stimulation did lead to the significant enrichment of STAT2 as a biotinylated factor in the close environment of BRD9 (Fig 6E, Dataset EV3). These results were confirmed in independent proximity labeling, affinity purification, and Western blot experiments, where GLTSCR1 could also be validated as a constitutive and specific interactor of BRD9, while the association of STAT2 with BRD9 was only observed following IFN-α2 treatment (Fig 6F). This is reminiscent of a previous observation that the central catalytic BAF subunit, SMARCA4, can directly interact with STAT2 and that this interaction can be enhanced by IFN-α stimulation (Huang *et al*, 2002). Notably, A549 cells appear to express a severely truncated and non-functional SMARCA4 (Medina *et al*, 2008; Vangamudi *et al*, 2015; Dornfeld *et al*, 2018), and the SMARCA4 paralogue SMARCA2 may compensate for SMARCA4 deficiency in BAF complexes during antiviral responses (Dornfeld *et al*, 2018). Together, these data suggest a functional interaction between BRD9-containing ncBAF complexes and STAT2 following IFN stimulation that likely contributes to driving ISG expression.

Discussion

Herein, we describe the identification and characterization of BRD9 as a host factor required for the efficient expression of a subset of ISGs and for the full antiviral activity of IFN. Mechanistically, BRD9

appears to act downstream of cytoplasmic JAK-STAT signaling and STAT protein nuclear translocation and likely impacts the IFN-induced transcription of ISGs following its proximal association at ISG promoters with nuclear STAT2-containing transcription factor complexes (i.e., the whole activated ISGF3 complex of STAT1, STAT2, and IRF9). BRD9 is a defining member of the ncBAF

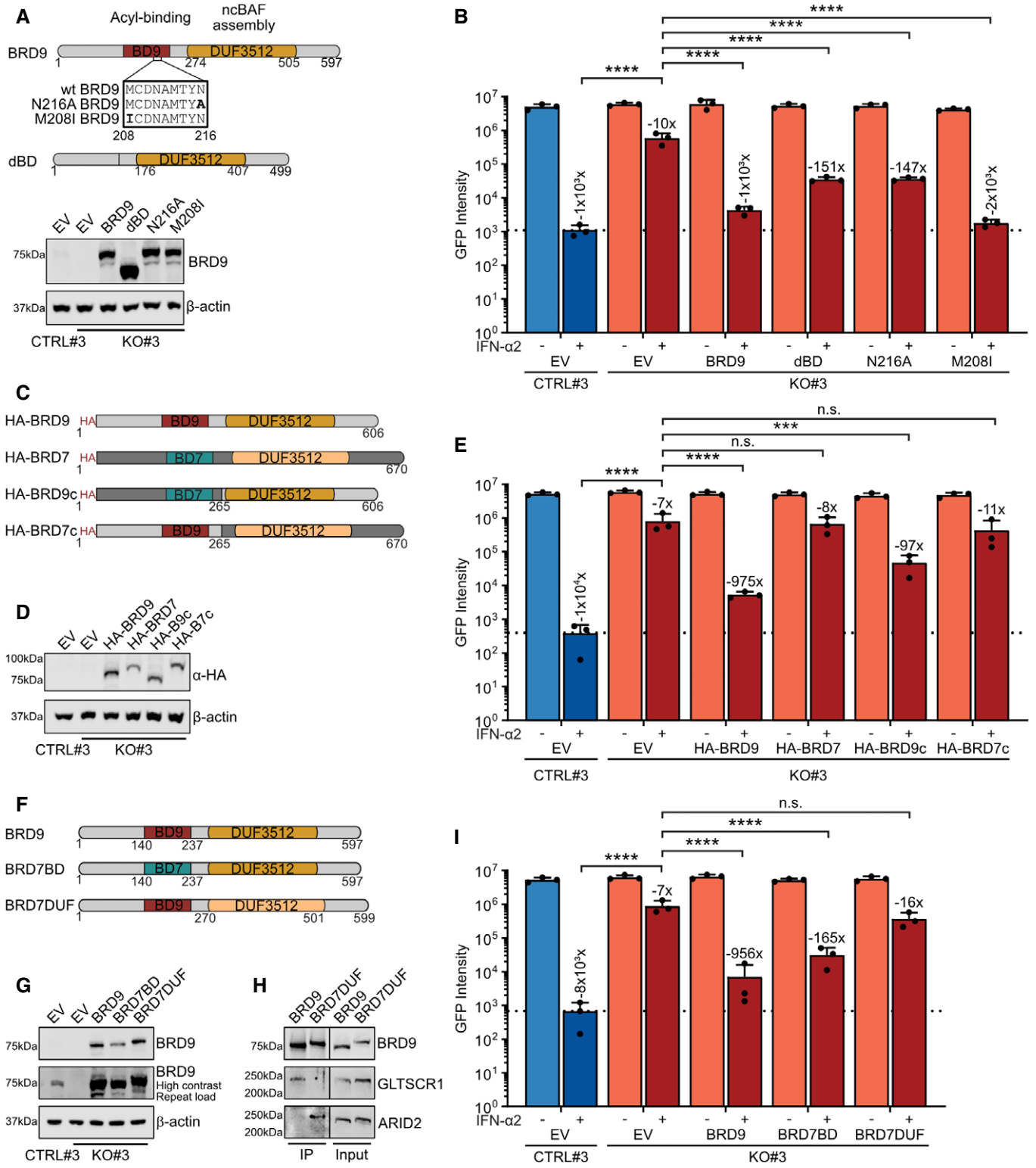

Figure 5.

Figure 5. BRD9 function requires its acetyl-binding activity and unique DUF3512 scaffolding domain.

A Top: schematic representation of wild-type (wt) human BRD9 and selected mutants, highlighting the acyl-binding bromodomain (BD9) and the DUF3512 domain responsible for ncBAF assembly. Numbers represent amino acid residues. The box highlights BD9 positions 208–216, which include residues critical for acetyl (N216) or butyryl (M208) binding. dBD is an engineered BRD9 variant lacking the entire bromodomain (residues 140–237). Bottom: Western blot analysis of CTRL#3 or BRD9-KO#3 cells stably transduced with lentiviruses expressing empty vector (EV), or wt and mutant BRD9 constructs.

B The various CTRL#3 or BRD9-KO#3 cells described in (A) were stimulated with 1,000 IU/ml of IFN-α2 for 16 h prior to infection with VSV-GFP at an MOI of 0.6 PFU/cell. Total integrated green fluorescent intensities were determined using the Incucyte live-cell analysis system at 48 h post-infection.

C Schematic representation of HA-tagged wt human BRD9, BRD7, and selected chimeric mutants. BD7 is the BRD7 bromodomain. Numbers represent amino acid residues of the final constructs.

D Western blot analysis of CTRL#3 or BRD9-KO#3 cells stably transduced with lentiviruses expressing empty vector (EV), or HA-tagged wt and chimeric mutant constructs described in (C).

E The various CTRL#3 or BRD9-KO#3 cells described in (D) were stimulated and infected as described in (B).

F Schematic representation of wt human BRD9, and selected chimeric mutants with domains from BRD7. Numbers represent amino acid residues of the final constructs.

G Western blot analysis of CTRL#3 or BRD9-KO#3 cells stably transduced with lentiviruses expressing empty vector (EV), or wt and chimeric constructs described in (F).

H Western blot analysis of input lysates and anti-BRD9 immunoprecipitations (IPs) from cells described in (G) expressing wt BRD9 or the chimeric BRD7DUF. The indicated proteins were detected with specific antibodies. Data are representative of two biological replicates.

I The various CTRL#3 or BRD9-KO#3 cells described in (G) were stimulated and infected as described in (B).

Data information: For (B), (E), and (I), data represent means and standard deviations from $n = 3$ biological experiments (individual data points shown). Numbers above IFN-α2-treated bars indicate their approximate difference to the respective untreated conditions. Dotted lines are a visual guide for minimum virus replication in control cells in the presence of IFN-α2. Statistical significance was determined by 1-way ANOVA on log-transformed intensity values (***$P < 0.001$; ****$P < 0.0001$; n.s. not significant). See also Fig EV5.
Source data are available online for this figure.

complex, and its C-terminal DUF3512 domain is essential for recruiting a key component, GLTSCR1/1L, into this complex. We found that switching the recruitment function of BRD9 from GLTSCR1/1L to ARID2 (a PBAF complex component), using a previously established domain swap technique (Michel *et al*, 2018), compromised the ability of BRD9 to promote the antiviral effects of IFN, suggesting an important and specific role for the ncBAF complex as a whole in the transcription-promoting activity of IFN. In support of this, we note that *GLTSCR1*, like *BRD9*, was also enriched in a separate screen to identify positive regulators of antiviral ISG expression in response to the type III IFN, IFN-λ (Lumb *et al*, 2017), a finding that we further observed with type I IFN-α using siRNAs. While some components of the canonical BAF and PBAF complexes (e.g., SMARCB1/BAF47 and ARID2/BAF200), as well as the central SMARCA4/BRG1 subunit, have previously been implicated in promoting specific ISG transcription in knockdown experiments (Huang *et al*, 2002; Liu *et al*, 2002; Cui *et al*, 2004; Yan *et al*, 2005; Patel *et al*, 2013; Marie *et al*, 2018), no other BAF or PBAF exclusive components were enriched in our genome-scale knockout screen, and siRNAs targeting the PBAF-specific BRD7 and ARID2 also failed to limit the antiviral action of IFN in our experiments. This could indicate that these canonical BAF factors are essential for cell viability, at least in the A549 cell line used here, or are already non-functional, as is reported for SMARCA4 (Medina *et al*, 2008; Vangamudi *et al*, 2015; Dornfeld *et al*, 2018). It is also possible that distinct BAF complexes differentially regulate specific ISG subsets in different cell types depending upon epigenetic factors or subunit expression levels, such that the presence of specific BAF complex compositions within cells actively shapes their individual ISG profiles in response to IFN. Why such distinct transcription regulatory mechanisms might be required in the IFN response, are gene specific, or involve different BAF complexes is currently unclear. Furthermore, it remains to be determined why such an additional level of regulation beyond formation of the canonical ISGF3 complex should be necessary for specific ISGs. Nevertheless, our findings here indicate that BRD9 is important, overall, for the antiviral ISG response (and can be targeted for inhibition) in a range of primary and transformed cells. Indeed, taken together with previous independent screening data (Lumb *et al*, 2017), the whole ncBAF complex appears to play a specific role in selected ISG expression in different cell types in response to both type I and III IFNs.

BRD9 function requires an intact bromodomain, and the ability to bind acetylated lysines is necessary for its promotion of IFN-stimulated antiviral activity. Presumably, this mediates the recruitment of the entire ncBAF complex to a specific target that remains to be elucidated, but which is likely to be acetylated histone tails (Flynn *et al*, 2015). Thus, the simplest interpretation of our findings, which is consistent with a previously published model of BAF complex association with the promoters of regulated genes (Cui *et al*, 2004), is that ncBAF constitutively localizes to some key gene promoters (including critical ISGs) via the acetyl-binding property of BRD9, where this complex functions to increase chromatin accessibility and thereby "prime" maximal ISG induction following IFN stimulation (Fig 7). We currently favor this model, as our proximity labeling proteomic assays did not reveal dramatic changes in the BRD9 interactome that might have indicated IFN-stimulated recruitment of BRD9 to new genomic sites. Rather, our data suggest recruitment of the STAT2-containing ISGF3 transcription factor complex to ISG promoters already harboring BRD9 and ncBAF, which is in line with other reports (Huang *et al*, 2002). However, we cannot rule out a more nuanced mechanism, or one that includes specific IFN-stimulated recruitment of BRD9/ncBAF to a subset of some ISG promoters that exhibit a particular epigenetic state, where ncBAF then impacts chromatin accessibility to promote STAT2/ISGF3 binding and/or activity. In addition, our proteomic experiments confirmed the previously described interaction of BRD4 with the ncBAF complex (Rahman *et al*, 2011; Alpsoy & Dykhuizen, 2018; Gatchalian *et al*, 2018), and BRD4 can mediate the recruitment of ncBAF subunits to chromatin in a bromodomain-dependent manner (Gatchalian *et al*, 2018). Furthermore, BRD4 itself has been

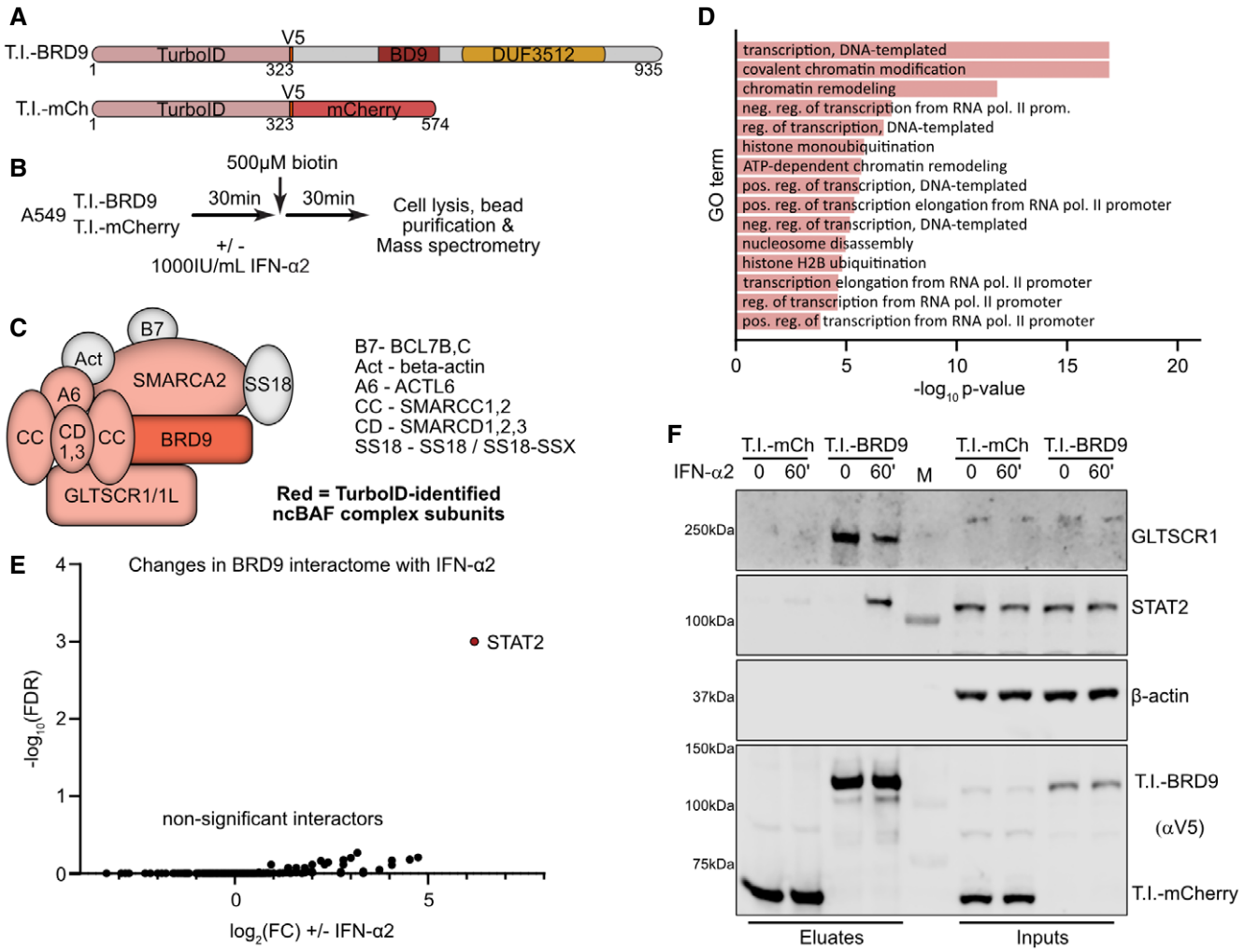

Figure 6. Interferon induces the close proximity of BRD9 with STAT2.

A Schematic representation of TurboID-tagged (T.I.) mCherry (negative control) and TurboID-tagged BRD9. V5 indicates the location of a V5-tag. Numbers represent amino acid residues of the final constructs. Both constructs were stably expressed in A549 cells.

B Overview of the proximity labeling workflow: interactomes of T.I.-mCherry or T.I.-BRD9 were determined in the presence/absence of a 60 min stimulation with 1,000 IU/ml of IFN-α2 and 500 µM biotin for 30 min.

C Schematic of the non-canonical BAF (ncBAF) complex, with factors identified with high confidence (SaintExpress Score ≥ 0.99) by proximity labeling to be specific interactors of BRD9 (as compared to mCherry) colored in red.

D GO term analysis of the 145 interactors identified to be specific to BRD9.

E Comparative BRD9 interactome analysis in the presence/absence of a 60 min stimulation with 1,000 IU/ml of IFN-α2. Note that FDR for STAT2 was 0, but has been set to 0.001 for visualization purposes.

F Western blot analysis of samples from independent small-scale streptavidin purifications (termed "Eluates") following the proximity labeling approach outlined in (B). The indicated proteins were detected with specific antibodies. M indicates the marker lane. Data are representative of at least two biological replicates.

Source data are available online for this figure.

implicated in the transcriptional regulation of ISGs (Patel *et al*, 2013; Marie *et al*, 2018), and IFN-induced chromatin recruitment mechanisms have been described in this context (Huang *et al*, 2002; Patel *et al*, 2013). Thus, the functional interplay between BRD9 and BRD4 remains to be further investigated, perhaps along with additional known targets of the BRD9 bromodomain, such as acetylated RAD54 (Zhou *et al*, 2020), acetylated CCAR2 (Rajendran *et al*, 2019), and the acetylated vitamin D receptor (VDR) (Wei *et al*, 2018). In this context, we note that VDR also has a proposed role in regulating the JAK-STAT pathway and IFN-mediated STAT1-dependent ISG responses (Lange *et al*, 2014).

An important outcome of our study was the observation that small-molecule-mediated degradation of BRD9, using dBRD9-A, limits IFN-induced expression of certain ISGs in multiple cell types. This finding could have implications for the consideration of BRD9 as a viable therapeutic target in the treatment of some autoinflammatory interferonopathies (Zhang *et al*, 2015; Meuwissen *et al*, 2016; Rodero & Crow, 2016; Rodero *et al*, 2017; Duncan *et al*, 2019;

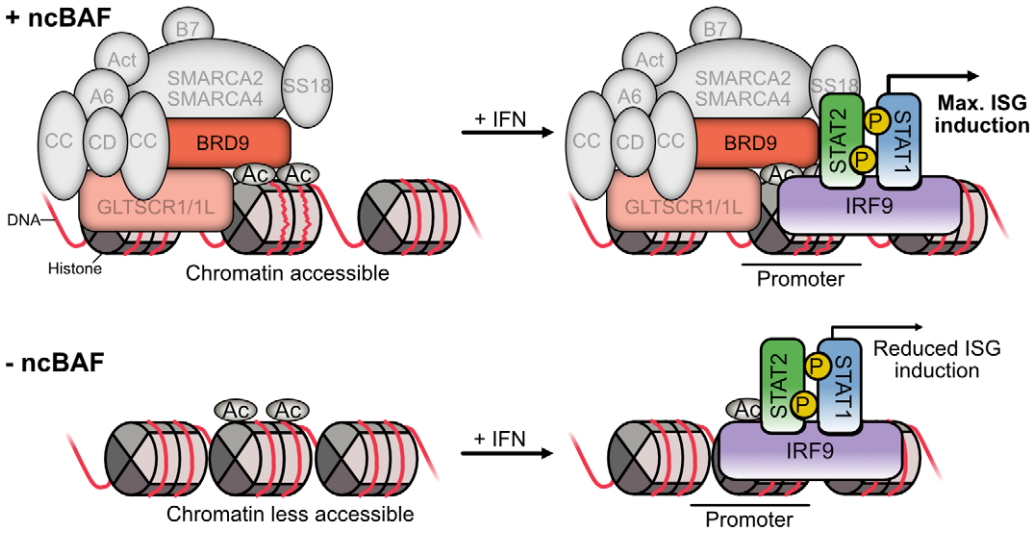

Figure 7. Hypothetical model of BRD9 and ncBAF function at selected interferon-stimulated gene promoters.

We hypothesize that the ncBAF complex is localized to the promoters of regulated genes by the interaction of the BRD9 bromodomain with histone acetylation marks. ncBAF activity may maintain the chromatin in an open state, thus enabling the efficient binding of ISGF3 complexes to ISRE sequences following IFN stimulation. Thus, maximal induction of ISG transcription may be "primed" to enhance downstream antiviral activity. In the absence of BRD9 (through genetic loss or targeted degradation with small molecules), ncBAF is removed from promoter regions, which may increase chromatin compaction and result in less efficient transcriptional activation of ISGs following IFN stimulation.

Kong *et al*, 2020; Martin-Fernandez *et al*, 2020; Rice *et al*, 2020), particularly under specific circumstances where broad targeting of JAK-mediated signaling may not be appropriate. Furthermore, we also note that BRD9 inhibition (or degradation) is an attractive therapeutic aim for the treatment of several cancers (Brien *et al*, 2018; Mashtalir *et al*, 2018; Hu *et al*, 2019). Therefore, our data should also raise awareness that, in such applications, drugs targeting BRD9 may have the undesirable side effect of limiting the effectiveness of endogenous host innate antiviral IFN responses, thereby potentially increasing the susceptibility of individuals to some infections.

Materials and Methods

Cells and compounds

293T, A549, MDCK, Huh-7, U87MG, Calu-3, Hep2, and mouse 3T3 cells (all originally from ATCC) were maintained in Dulbecco's modified Eagle's medium (DMEM) (Life Technologies) supplemented with 10% (v/v) fetal calf serum (FCS), 2 mM L-glutamine, 100 units/ml penicillin, and 100 μg/ml streptomycin (Gibco Life Technologies). MRC-5 cells (originally from ATCC) were cultured in minimum essential medium Eagle (MEM) supplemented with 10% (v/v) FCS, 100 units/ml penicillin, 100 μg/ml streptomycin, 2 mM L-glutamine (Gibco Life Technologies), and 1% (v/v) non-essential amino acids (Life Technologies). Primary human tracheobronchial epithelial cells were purchased from Lonza and maintained in supplemented basal medium (Promocell). The original A549/pr (ISRE).eGFP cells were kindly provided by Rick Randall and Catherine Adamson (University of St Andrews, UK) (Stewart *et al*, 2014). The A549/pr(ISRE).eGFP.A1 sub-clone was subsequently obtained by limiting dilution of FACS-sorted eGFP-positive cells following 2 rounds of IFN-α2 (Novus Biologicals) stimulation (1,000 IU/ml for 16 h). The A549/pr(ISRE).eGFP.A1 sub-clone was found to induce high and homogenous levels of eGFP following IFN-α2 stimulation as assessed by the IncuCyte live-cell analysis system (Sartorius) and flow cytometry (see below). The A549-2D8 sub-clone was obtained by limiting dilution of A549 cells and subsequent selection of a clone that exhibited high IFN-induced antiviral activity against IAV. Cell lines were not authenticated, but were routinely tested for mycoplasma contamination (GATC, Germany). None of the cell lines used ever tested positive for mycoplasma. Cycloheximide was purchased from Sigma-Aldrich. dBRD9-A (Brien *et al*, 2018) was custom-synthesized by ChemPartner, dissolved in DMSO, and used at the indicated concentration. Recombinant human TNF-α was purchased from Preprotech. Cell viability was measured as indicated using the CellTiterGlo (Promega) assay kit, following the manufacturer's instructions.

Viruses and infections

Propagation, titration, and use of wild-type influenza A virus (IAV; WSN/33 strain) have been described previously (Spieler *et al*, 2020). VSV-GFP was a kind gift from Peter Palese (Icahn School of Medicine, New York, USA). HSV1-GFP was kindly provided by Jovan Pavlovic (University of Zurich, Switzerland) (Crameri *et al*, 2018). VSV-G pseudotyped HIV1-GFP (NHGΔenvGFP) was generated as previously described using plasmids from Sam Wilson (University of Glasgow, UK) (Busnadiego *et al*, 2014; Kane *et al*, 2016). For IAV infections, approximately 1×10^5 cells were treated or not with 1,000 IU/ml of IFN-α2 for 16 h prior to infection at the indicated multiplicity of infection (MOI) in PBS supplemented with 0.3% BSA, 1 mM Ca^{2+}/Mg^{2+}, 100 units/ml penicillin, and 100 μg/

ml streptomycin. After 1 h, infected cells were washed three times with PBS and then overlaid with DMEM supplemented with 0.1% FBS, 0.3% BSA, 20 mM HEPES, 100 units/ml penicillin, and 100 μg/ml streptomycin. Supernatants were collected at the indicated times post-infection and titrated by standard plaque assay on MDCK cells. For the GFP-encoding reporter viruses (VSV-GFP, HSV1-GFP, and pseudotyped HIV1-GFP), approximately 1.5–3 × 10^4 cells/well in 96-well plates were treated with DMSO, dBRD9-A, and/or IFN-α2 (or universal IFN; PBL Assay Science) as indicated, washed once in PBS, then incubated with the appropriate amount of virus diluted in FluoroBrite DMEM (Life Technologies) medium supplemented with 2% (v/v) FCS, 2 mM L-glutamine, 100 units/ml penicillin, and 100 μg/ml streptomycin. Infections were monitored in live cells via GFP expression using the Incucyte live-cell analysis system (Sartorius) for 24–72 h. Total Green Integrated Intensity (Green Calibrated Unit × μm²/image) values were exported at the indicated time points.

CRISPR screening

The full human GeCKOv2 CRISPR knockout pooled library (Addgene #1000000048, a gift from Feng Zhang) was used for genome-scale screening (Sanjana *et al*, 2014), essentially as described (Joung *et al*, 2017). Briefly, the GeCKOv2 plasmid library with 6 guide RNAs per human gene was propagated in Endura ElectroCompetent cells (Lucigen), and lentivirus stocks were generated by co-transfecting 293T cells with the GeCKOv2 plasmid library, pMD2.G and psPAX2 (Addgene plasmids #12259 and #12260, gifts from Didier Trono) at a ratio of 4:2:1 (GeCKOv2: psPAX2:pMD2.G). After 48 h, lentivirus-containing supernatants were clarified by low-speed centrifugation and filtration through a 0.45 μm filter prior to storage at −80°C. Following titration of the lentiviral library, 1 × 10^8 A549/pr(ISRE).eGFP.A1 cells were transduced at a multiplicity of infection (MOI) 0.3 FFU/cell and selected with 1 μg/ml puromycin for 14 days. Surviving cells were stimulated with 1,000 IU/ml of IFN-α2 (Novus Biologicals) for 16 h prior to FACS-based sorting of eGFP-negative cells (Cytometry Facility, University of Zurich), which were then plated into new flasks and allowed to recover. DNA was subsequently isolated from both sorted and non-sorted cells as previously described (Chen *et al*, 2015). Briefly, cells were lysed in 50 mM Tris pH 8, 50 mM EDTA, and 1% SDS, supplemented with proteinase K (Qiagen), and incubated overnight at 55°C. RNA was then digested by addition of RNAseA (Qiagen) for 30 min at 37°C. Pre-cooled 7.5 M ammonium acetate was added to a final concentration of 1.75 M, and remaining impurities were removed by centrifugation. DNA was finally precipitated by addition of isopropanol, washed once in 70% ethanol, and resuspended in a 5 mM Tris buffer. Integrated sgRNAs were PCR-amplified by an initial 14 cycles using 7 μg/50 μl isolated DNA as template. Reactions were pooled and subjected to a second round of 26 PCR cycles using described primers (Joung *et al*, 2017). All PCRs were performed using Kapa HiFi Hotstart polymerase (Kapa Biosystems). Amplicons were separated on a 2% agarose gel, column-purified (Qiagen), and sequenced on an Illumina NextSeq500 at the Functional Genomics Center Zurich. Data analysis from two biologically independent CRISPR screen experiments, including unsorted control samples, was performed using the PinAPL-Py platform (Spahn *et al*, 2017) and the adjusted robust-rank aggregation (αRRA) algorithm with default settings (*P*-value = 0.01; 1,000 permutations).

siRNA transfections

ON-TARGETplus SMARTpool siRNAs targeting IRF9, BRD9, GLTSCR1, BRD7, and ARID2 were purchased from Horizon Discovery. A custom non-targeting scrambled control siRNA (scrambled1777; siSCR) has been described previously (Karakus *et al*, 2019). Reverse transfection of A549-2D8 cells was performed in 96-well plates 32 h prior to the indicated treatment using approximately 8 × 10^3 cells/well, 30 nM final concentration of each siRNA, and Lipofectamine RNAiMAX Transfection Reagent (Thermo Fisher Scientific).

Generation of knockout (KO) cells

Gene knockouts were generated using either the lentiCRISPRv2 system (Addgene plasmid #52961, a gift from Feng Zhang) (Sanjana *et al*, 2014) using the methods described above and specific sgRNA-encoding oligos (Table EV1), or a ribonucleoprotein (RNP)-based system described previously (Domingues *et al*, 2019). Briefly, pre-assembled RNP complexes (see Table EV1 for crRNA sequences) were delivered into cells by reverse transfection with RNAiMax (Thermo Fisher Scientific), and individual cell clones were generated by limiting dilution. Genotypes of selected clones were determined by amplification of the appropriate genomic region and subsequent NGS. Oligo sequences are deposited in Table EV1.

Flow cytometry analysis

A549/pr(ISRE).eGFP.A1 cells were transduced at high MOI (> 10 FFU/cell) with a pool of three lentiviruses encoding sgRNAs targeting the indicated factors. After 48 h, selection of transduced cells was started with 1 μg/ml puromycin and maintained for at least 10 days. Transduced cells were then treated with 1,000 IU/ml IFN-α2 for 16 h, and eGFP expression was quantified in the FITC channel using a BD FACSCanto II.

Plasmids and lentiviruses

cDNAs encoding BRD7, BRD9, BRD9-dBD, and BRD9-N216A were PCR-amplified from existing vectors (Addgene plasmids #65379 (Gong *et al*, 2015) and #75114-6 (Hohmann *et al*, 2016); gifts from Kyle Miller and Christopher Vakoc) and cloned into pLVX-IRES-Puro (Takara) via XhoI/NotI or EcoRI/NotI sites. The indicated chimeras of BRD7 and BRD9 were generated by overlapping PCRs or InFusion (Takara). Remaining variants of BRD9 were generated by overlap-extension PCR using Q5 Hot Start High-Fidelity (NEB). TurboID-V5 constructs were generated by first sub-cloning TurboID from an existing vector (Addgene plasmid #107169 (Branon *et al*, 2018), a gift from Alice Ting), together with the V5 linker sequence, into the multiple cloning site of pLVX-IRES-Puro, followed by insertion of BRD9, or mCherry, via EcoRI/NotI sites. All new constructs were authenticated by DNA sequencing. All oligo sequences used for cloning and mutagenesis are available in Table EV1. To generate polyclonal cell lines expressing the gene of interest, lentiviral stocks were initially prepared by co-transfecting 293T cells with each pLVX-IRES-Puro-based plasmid, together with pMD2.G and psPAX2.

Lentiviral supernatants were harvested ~60 h post-transfection, filtered through a 0.45μm filter, and aliquoted for storage at −80°C. Cells were transduced with the appropriate lentivirus stock for 48 h in the presence of 8 μg/ml of polybrene (Millipore) prior to selection with puromycin.

RT–qPCR analyses

Around 1×10^5 cells were treated as indicated prior to lysis and RNA isolation using the ReliaPrep™ RNA Miniprep kit (Promega). Approximately 1 μg of total RNA was reverse transcribed into cDNA using SuperScript III (Invitrogen) and an oligo(dT) primer (Thermo Fisher). Transcripts were detected using specific primers (Table EV1), the Fast EvaGreen qPCR Master Mix (Biotium), and an ABI7300 Real-Time PCR System. Relative gene expression was determined with the $\Delta\Delta C_t$ method, using GAPDH for normalization.

Transcriptome analysis

RNA was extracted as described above, and libraries from three biologically independent experiments were prepared and analyzed by the Functional Genomics Center Zurich following the Illumina TruSeq stranded mRNA protocol. Briefly, the quality of RNA and final libraries was first determined using the Agilent 4200 TapeStation System. Libraries were then pooled equimolarily and sequenced on an Illumina NovaSeq6000 sequencer (single-end 100 bp) with a depth of around 20 million reads per sample. Reads were quality-checked with FastQC. Sequencing adapters were removed with Trimmomatic (Bolger *et al*, 2014) and aligned to the reference genome and transcriptome of *Homo sapiens* (GENCODE, GRCh38.p10, release 91) with STAR v2.7.3 (Dobin *et al*, 2013). Distribution of the reads across genomic isoform expression was quantified using the R package GenomicRanges (Lawrence *et al*, 2013) from Bioconductor version 3.10. Minimum mapping quality, as well as minimum feature overlaps, was set to 10. Multi-overlaps were allowed. Differentially expressed transcripts were identified using the R package edgeR (Robinson *et al*, 2010) from Bioconductor version 3.10, using a generalized linear model (glm) regression, a quasi-likelihood (QL) differential expression test, and trimmed means of M-values (TMM) normalization.

Western blotting

Generally, samples were prepared in urea disruption buffer (6 M urea, 2 M β-mercaptoethanol, and 4% SDS), and DNA was sheared either by passing through a 29G needle or by sonication (Branson 250, 12×0.5/1s pulses at 10% amplitude). For detection of BRD9 in A549 cells, lysates were prepared on ice for 20 min in RIPA buffer (50 mM Tris–HCl pH 8.0, 150 mM NaCl, 0.1% SDS, 1% sodium deoxycholate, 1% Triton X-100), DNA sheared as described above, and protein concentration measured by BCA assay (Pierce Thermo Fisher). At least 30 μg of protein was loaded onto gels to detect endogenous BRD9. Proteins were separated by SDS–PAGE on NuPAGE Novex or Bolt 4–12% Bis-Tris gels (Invitrogen) prior to transfer to Protran nitrocellulose membranes (Amersham) at 30 V for 90 min. Proteins were detected using the following primary antibodies: β-actin (Santa Cruz, sc-47778); MxA (kind gift from Jovan Pavlovic, University of Zurich, Switzerland); FLAG M2 (Sigma, F1804); BRD9 (Bethyl Laboratories, A303-781A-M); BRD7 (Cell Signaling Technology, D9K2T); HA (Cell Signaling Technology, 3724); V5 (Bio-Rad, MCA1360); STAT1 (Cell Signaling Technology, 14994S); pSTAT1 (Cell Signaling Technology, 9167S); STAT2 (Santa Cruz, sc-1668); GLTSCR1 (Santa Cruz, sc-515086); JAK1 (BD Bioscience, 610231); pJAK1 (Cell Signaling Technology, 74129); ARID2 (Santa Cruz, sc-166117). Signal was detected using the LiCOR system or ECL.

Immunofluorescence microscopy

5×10^5 cells were seeded onto coverslips in 12-well plates and treated the next day for the indicated time with 1,000 IU/ml IFN-α2, prior to fixation with 3.7% paraformaldehyde (Sigma-Aldrich) for 10 min at room temperature. Coverslips were washed once in PBS, permeabilized with 1% Triton X-100 (in PBS) for 10 min, then washed a further three times in PBS. Blocking was performed by incubating coverslips for 1 h with PBS + 2% BSA (v/v) at room temperature. Following incubation of cells with pSTAT1 and STAT1 antibodies (Cell Signaling 9167S and 14994S), cells were washed three times with PBS before incubation with the appropriate secondary antibody and a further three washes in PBS. As necessary, DNA was stained by incubating with DAPI (Sigma-Aldrich) for 5 min. Following a final three washes in PBS and two washes in ddH_2O, coverslips were mounted onto slides using ProLong Gold Antifade (Life Technologies). Cells were imaged using the Leica DM IL LED Fluo microscope (Leica Microsystems), using the LasX software.

Immunoprecipitation (IP) assays

~5×10^6 of the indicated cells were washed once in PBS prior to lysis on ice in IP buffer (50 mM Tris–HCl pH 7.5, 150 mM NaCl, 1 mM EDTA, and 1% Triton X-100) supplemented with complete protease inhibitors (Roche). DNA was sheared by sonication (Branson 250, 30× 0.5/1s pulses at 10% amplitude) and removed by addition of Benzonase (Millipore) for 1 h at room temperature. Lysates were cleared by centrifugation at 16,000 *g* for 10 min at 4°C, and a fraction was taken to represent input. The remainder of the soluble sample was incubated with 5 μg of anti-BRD9 antibody (see above) for 16 h at 4°C with constant rotation. Antibody–protein complexes were captured with Dynabeads Protein G (Thermo Fisher Scientific) for 30 min at room temperature with constant rotation. Following three bead washes in IP buffer, samples were prepared in Laemmli buffer and analyzed by Western blot.

TurboID proximity labeling

Approximately 5×10^5 cells stably expressing the indicated TurboID-V5-fusion proteins were treated as described prior to the addition of 500 μM biotin (Sigma-Aldrich) for 30 min. Cells were subsequently washed five times in PBS, before lysis on ice for 20 min in RIPA buffer supplemented with complete protease inhibitors (Roche). DNA was sheared as described above and removed by addition of Benzonase (Millipore) for 1 h at 4°C. Lysates were cleared by centrifugation at 16,000 *g* for 10 min at 4°C, and a fraction was taken to represent input. The remainder of the sample was processed as described (Hung *et al*, 2016) with slight modifications: briefly, lysates were incubated with streptavidin magnetic beads (Pierce Thermo Fisher) for 1 h at room temperature on a rotator to

bind biotinylated proteins. Samples were then washed twice in RIPA buffer, once in 1 M KCl, once in 0.1 M Na_2CO_3, and once in freshly prepared 1 M urea, 10 mM Tris–HCl pH 8.0. For proteomic analysis, samples were then washed three times in freshly prepared ABC buffer (50 mM ammonium bicarbonate). For Western blot analysis, samples were washed three times in RIPA buffer. Proteomic sample preparation and liquid chromatography–mass spectrometry analysis was performed by the Functional Genomics Center Zurich. Proteins were identified using FragPipe (v12.2) and the MSFragger—Ultrafast Proteomics Search Engine (Kong *et al*, 2017). Spectra were searched against a canonical Swiss-Prot *Homo sapiens* proteome database (taxonomy 9606, version from 02/2020), concatenated to its reversed decoyed fasta database. Methionine oxidation was set as variable modification, and enzyme specificity was set to trypsin allowing a maximum of two missed cleavages. A fragment ion mass tolerance of 0.1 Da and a precursor mass tolerance of 50 PPM were set. The SaintExpress algorithm (Teo *et al*, 2014) was utilized to analyze the spectral count shotgun MS data between samples, with the following settings applied by the CRAPome websuite: lowMode = 0; minFold = 1; normalize = 0. The raw mass spectrometry proteomics data have been deposited to the ProteomeXchange Consortium via the PRIDE (Perez-Riverol *et al*, 2019) partner repository with the dataset identifier PXD026926.

Gene ontology (GO) analyses

GO analyses of identified interactors in TurboID experiments, or differential expressed genes in transcriptomics experiment, were performed using medium stringency settings in DAVID (da Huang *et al*, 2009), using all human genes as background. We excluded BRD9 from the analysis of the proteomics data as it was the bait.

Statistical analyses

Statistical analyses were performed in GraphPad Prism 9.0.0. FACS MFI data were analyzed by pairwise comparison using an unpaired *t*-test. Data using virus titers or eGFP intensities were $\log_{10}$-transformed and analyzed by unpaired 2-tailed *t*-test or 1-way ANOVA for comparison of multiple conditions. For RT–qPCR data, ΔC_t values were analyzed by unpaired 2-tailed *t*-test.

Data availability

The datasets produced in this study are available in the following databases:

- RNA-Seq data: Gene Expression Omnibus GSE178640 (https://www.ncbi.nlm.nih.gov/geo/query/acc.cgi?acc=GSE178640).
- Mass spectrometry proteomics data: PRIDE PXD026926 (http://www.ebi.ac.uk/pride/archive/projects/PXD026926).

Expanded View for this article is available online.

Acknowledgements
We thank Michael Huber, Stefan Schmutz, Marie Lork, and Marie Pohl (University of Zurich, Switzerland) for helpful discussions and advice relating to practical aspects of this work. We are particularly grateful to Rick Randall and Catherine Adamson (University of St Andrews, UK) for provision of the original A549/pr(ISRE).eGFP cell line and to David Remillard (Scripps Research Institute, USA) for advice on dBRD9-A synthesis and use. We also acknowledge Kyle Miller, Peter Palese, Jovan Pavlovic, Alice Ting, Didier Trono, Christopher Vakoc, Sam Wilson, and Feng Zhang for providing essential reagents. Amplicon sequencing, transcriptome analyses, and proteome analyses were performed with support from the Functional Genomics Center Zurich. Flow cytometry and FACS were performed with support from the Cytometry Facility, University of Zurich. The synopsis figure was created with BioRender.com. The research leading to these results received funding from the Swiss National Science Foundation (grant 31003A_182464 to BGH).

Author contributions
Conceptualization: JB, DE and BGH; Methodology and Investigation: JB, DE, NKM, IB, EM, NS, SS, PPP and WW-LW; Resources: NKM and SS; Writing and Visualization: JB, DE and BGH; Supervision: MS and BGH; Funding Acquisition and Project Administration: BGH.

Conflict of interest
The authors declare that they have no conflict of interest.

References

Duncan CJA, Thompson BJ, Chen R, Rice GI, Gothe F, Young DF, Lovell SC, Shuttleworth VG, Brocklebank V, Corner B *et al* (2019) Severe type I interferonopathy and unrestrained interferon signaling due to a homozygous germline mutation in STAT2. *Sci Immunol* 4: eaav7501

Alpsoy A, Dykhuizen EC (2018) Glioma tumor suppressor candidate region gene 1 (GLTSCR1) and its paralog GLTSCR1-like form SWI/SNF chromatin remodeling subcomplexes. *J Biolo Chem* 293: 3892 – 3903

Alsohime F, Martin-Fernandez M, Temsah M-H, Alabdulhafid M, Le Voyer T, Alghamdi M, Qiu X, Alotaibi N, Alkahtani A, Buta S *et al* (2020) JAK inhibitor therapy in a child with inherited USP18 deficiency. *N Engl J Med* 382: 256 – 265

Au-Yeung N, Horvath CM (2018) Histone H2A.Z suppression of interferon-stimulated transcription and antiviral immunity is modulated by GCN5 and BRD2. *iScience* 6: 68 – 82

Bhattacharya S, Eckner R, Grossman S, Oldread E, Arany Z, D'Andrea A, Livingston DM (1996) Cooperation of Stat2 and p300/CBP in signalling induced by interferon-alpha. *Nature* 383: 344 – 347

Bolger AM, Lohse M, Usadel B (2014) Trimmomatic: a flexible trimmer for Illumina sequence data. *Bioinformatics* 30: 2114 – 2120

Branon TC, Bosch JA, Sanchez AD, Udeshi ND, Svinkina T, Carr SA, Feldman JL, Perrimon N, Ting AY (2018) Efficient proximity labeling in living cells and organisms with TurboID. *Nat Biotechnol* 36: 880 – 887

Brien GL, Remillard D, Shi J, Hemming ML, Chabon J, Wynne K, Dillon ET, Cagney G, Van Mierlo G, Baltissen MP *et al* (2018) Targeted degradation of BRD9 reverses oncogenic gene expression in synovial sarcoma. *Elife* 7: e41305

Busnadiego I, Kane M, Rihn SJ, Preugschas HF, Hughes J, Blanco-Melo D, Strouvelle VP, Zang TM, Willett BJ, Boutell C *et al* (2014) Host and viral determinants of Mx2 antiretroviral activity. *J Virol* 88: 7738 – 7752

Chang HM, Paulson M, Holko M, Rice CM, Williams BR, Marie I, Levy DE (2004) Induction of interferon-stimulated gene expression and antiviral responses require protein deacetylase activity. *Proc Natl Acad Sci USA* 101: 9578 – 9583

Chen S, Sanjana N, Zheng K, Shalem O, Lee K, Shi Xi, Scott D, Song J, Pan J, Weissleder R *et al* (2015) Genome-wide CRISPR screen in a mouse model of tumor growth and metastasis. *Cell* 160: 1246 – 1260

Crameri M, Bauer M, Caduff N, Walker R, Steiner F, Franzoso FD, Gujer C, Boucke K, Kucera T, Zbinden A *et al* (2018) MxB is an interferon-induced restriction factor of human herpesviruses. *Nat Commun* 9: 1980

Cui K, Tailor P, Liu H, Chen X, Ozato K, Zhao K (2004) The chromatin-remodeling BAF complex mediates cellular antiviral activities by promoter priming. *Mol Cell Biol* 24: 4476 – 4486

Dobin A, Davis CA, Schlesinger F, Drenkow J, Zaleski C, Jha S, Batut P, Chaisson M, Gingeras TR (2013) STAR: ultrafast universal RNA-seq aligner. *Bioinformatics* 29: 15 – 21

Domingues P, Eletto D, Magnus C, Turkington HL, Schmutz S, Zagordi O, Lenk M, Beer M, Stertz S, Hale BG (2019) Profiling host ANP32A splicing landscapes to predict influenza A virus polymerase adaptation. *Nat Commun* 10: 3396

Dornfeld D, Dudek AH, Vausselin T, Günther SC, Hultquist JF, Giese S, Khokhlova-Cubberley D, Chew YC, Pache L, Krogan NJ *et al* (2018) SMARCA2-regulated host cell factors are required for MxA restriction of influenza A viruses. *Sci Rep* 8: 2092

Duncan CJA, Randall RE, Hambleton S (2021) Genetic lesions of type I interferon signalling in human antiviral immunity. *Trends Genet* 37: 46 – 58

Flynn EM, Huang OW, Poy F, Oppikofer M, Bellon SF, Tang Y, Cochran AG (2015) A subset of human bromodomains recognizes butyryllysine and crotonyllysine histone peptide modifications. *Structure* 23: 1801 – 1814

Gatchalian J, Malik S, Ho J, Lee DS, Kelso TWR, Shokhirev MN, Dixon JR, Hargreaves DC (2018) A non-canonical BRD9-containing BAF chromatin remodeling complex regulates naive pluripotency in mouse embryonic stem cells. *Nat Commun* 9: 5139

Gnatovskiy L, Mita P, Levy DE (2013) The human RVB complex is required for efficient transcription of type I interferon-stimulated genes. *Mol Cell Biol* 33: 3817 – 3825

Gong F, Chiu L-Y, Cox B, Aymard F, Clouaire T, Leung JW, Cammarata M, Perez M, Agarwal P, Brodbelt JS *et al* (2015) Screen identifies bromodomain protein ZMYND8 in chromatin recognition of transcription-associated DNA damage that promotes homologous recombination. *Genes Dev* 29: 197 – 211

Hohmann AF, Martin LJ, Minder JL, Roe J-S, Shi J, Steurer S, Bader G, McConnell D, Pearson M, Gerstberger T *et al* (2016) Sensitivity and engineered resistance of myeloid leukemia cells to BRD9 inhibition. *Nat Chem Biol* 12: 672 – 679

Hu Z, Zhou J, Jiang J, Yuan J, Zhang Y, Wei X, Loo N, Wang Y, Pan Y, Zhang T *et al* (2019) Genomic characterization of genes encoding histone acetylation modulator proteins identifies therapeutic targets for cancer treatment. *Nat Commun* 10: 733

Huang M, Qian F, Hu Y, Ang C, Li Z, Wen Z (2002) Chromatin-remodelling factor BRG1 selectively activates a subset of interferon-alpha-inducible genes. *Nat Cell Biol* 4: 774 – 781

da Huang W, Sherman BT, Lempicki RA (2009) Systematic and integrative analysis of large gene lists using DAVID bioinformatics resources. *Nat Protoc* 4: 44 – 57

Hung V, Udeshi ND, Lam SS, Loh KH, Cox KJ, Pedram K, Carr SA, Ting AY (2016) Spatially resolved proteomic mapping in living cells with the engineered peroxidase APEX2. *Nat Protoc* 11: 456 – 475

Ivashkiv LB, Donlin LT (2014) Regulation of type I interferon responses. *Nat Rev Immunol* 14: 36 – 49

Joung J, Konermann S, Gootenberg JS, Abudayyeh OO, Platt RJ, Brigham MD, Sanjana NE, Zhang F (2017) Genome-scale CRISPR-Cas9 knockout and transcriptional activation screening. *Nat Protoc* 12: 828 – 863

Kalunian KC (2016) Interferon-targeted therapy in systemic lupus erythematosus: Is this an alternative to targeting B and T cells? *Lupus* 25: 1097 – 1101

Kane M, Zang TM, Rihn SJ, Zhang F, Kueck T, Alim M, Schoggins J, Rice CM, Wilson SJ, Bieniasz PD (2016) Identification of interferon-stimulated genes with antiretroviral activity. *Cell Host Microbe* 20: 392 – 405

Karakus U, Thamamongood T, Ciminski K, Ran W, Günther SC, Pohl MO, Eletto D, Jeney C, Hoffmann D, Reiche S *et al* (2019) MHC class II proteins mediate cross-species entry of bat influenza viruses. *Nature* 567: 109 – 112

Kolde R, Laur S, Adler P, Vilo J (2012) Robust rank aggregation for gene list integration and meta-analysis. *Bioinformatics* 28: 573 – 580

Kong AT, Leprevost FV, Avtonomov DM, Mellacheruvu D, Nesvizhskii AI (2017) MSFragger: ultrafast and comprehensive peptide identification in mass spectrometry-based proteomics. *Nat Methods* 14: 513 – 520

Kong X-F, Worley L, Rinchai D, Bondet V, Jithesh PV, Goulet M, Nonnotte E, Rebillat AS, Conte M, Mircher C *et al* (2020) Three copies of four interferon receptor genes underlie a mild type I interferonopathy in down syndrome. *J Clin Immunol* 40: 807 – 819

Lange CM, Gouttenoire J, Duong FH, Morikawa K, Heim MH, Moradpour D (2014) Vitamin D receptor and Jak-STAT signaling crosstalk results in calcitriol-mediated increase of hepatocellular response to IFN-alpha. *J Immunol* 192: 6037 – 6044

Lau JF, Nusinzon I, Burakov D, Freedman LP, Horvath CM (2003) Role of metazoan mediator proteins in interferon-responsive transcription. *Mol Cell Biol* 23: 620 – 628

Lawrence M, Huber W, Pages H, Aboyoun P, Carlson M, Gentleman R, Morgan MT, Carey VJ (2013) Software for computing and annotating genomic ranges. *PLoS Comput Biol* 9: e1003118

Lazear HM, Schoggins JW, Diamond MS (2019) Shared and Distinct Functions of Type I and Type III Interferons. *Immunity* 50: 907 – 923

Liu H, Kang H, Liu R, Chen X, Zhao K (2002) Maximal induction of a subset of interferon target genes requires the chromatin-remodeling activity of the BAF complex. *Mol Cell Biol* 22: 6471 – 6479

Lu Y, Stuart JH, Talbot-Cooper C, Agrawal-Singh S, Huntly B, Smid AI, Snowden JS, Dupont L, Smith GL (2019) Histone deacetylase 4 promotes type I interferon signaling, restricts DNA viruses, and is degraded via vaccinia virus protein C6. *Proc Natl Acad Sci USA* 116: 11997 – 12006

Lumb JH, Li Q, Popov LM, Ding S, Keith MT, Merrill BD, Greenberg HB, Li JB, Carette JE (2017) DDX6 represses aberrant activation of interferon-stimulated genes. *Cell Rep* 20: 819 – 831

Marie IJ, Chang HM, Levy DE (2018) HDAC stimulates gene expression through BRD4 availability in response to IFN and in interferonopathies. *J Exp Med* 215: 3194 – 3212

Martin-Fernandez M, Bravo García-Morato M, Gruber C, Murias Loza S, Malik MNH, Alsohime F, Alakeel A, Valdez R, Buta S, Buda G *et al* (2020) Systemic type I IFN inflammation in human ISG15 deficiency leads to necrotizing skin lesions. *Cell Rep* 31: 107633

Mashtalir N, D'Avino AR, Michel BC, Luo J, Pan J, Otto JE, Zullow HJ, McKenzie ZM, Kubiak RL, St. Pierre R *et al* (2018) Modular organization and assembly of SWI/SNF family chromatin remodeling complexes. *Cell* 175: 1272 – 1288.e20

Medina PP, Romero OA, Kohno T, Montuenga LM, Pio R, Yokota J, Sanchez-Cespedes M (2008) Frequent BRG1/SMARCA4-inactivating mutations in human lung cancer cell lines. *Hum Mutat* 29: 617 – 622

Mesev EV, LeDesma RA, Ploss A (2019) Decoding type I and III interferon signalling during viral infection. *Nat Microbiol* 4: 914 – 924

Meuwissen MEC, Schot R, Buta S, Oudesluijs G, Tinschert S, Speer SD, Li Z, van Unen L, Heijsman D, Goldmann T *et al* (2016) Human USP18 deficiency underlies type 1 interferonopathy leading to severe pseudo-TORCH syndrome. *J Exp Med* 213: 1163 – 1174

Michel BC, D'Avino AR, Cassel SH, Mashtalir N, McKenzie ZM, McBride MJ, Valencia AM, Zhou Q, Bocker M, Soares LMM *et al* (2018) A non-canonical SWI/SNF complex is a synthetic lethal target in cancers driven by BAF complex perturbation. *Nat Cell Biol* 20: 1410 – 1420

Nusinzon I, Horvath CM (2003) Interferon-stimulated transcription and innate antiviral immunity require deacetylase activity and histone deacetylase 1. *Proc Natl Acad Sci USA* 100: 14742 – 14747

Patel MC, Debrosse M, Smith M, Dey A, Huynh W, Sarai N, Heightman TD, Tamura T, Ozato K (2013) BRD4 coordinates recruitment of pause release factor P-TEFb and the pausing complex NELF/DSIF to regulate transcription elongation of interferon-stimulated genes. *Mol Cell Biol* 33: 2497 – 2507

Paulson M, Pisharody S, Pan L, Guadagno S, Mui AL, Levy DE (1999) Stat protein transactivation domains recruit p300/CBP through widely divergent sequences. *J Biol Chem* 274: 25343 – 25349

Paulson M, Press C, Smith E, Tanese N, Levy DE (2002) IFN-Stimulated transcription through a TBP-free acetyltransferase complex escapes viral shutoff. *Nat Cell Biol* 4: 140 – 147

Perez-Riverol Y, Csordas A, Bai J, Bernal-Llinares M, Hewapathirana S, Kundu DJ, Inuganti A, Griss J, Mayer G, Eisenacher M *et al* (2019) The PRIDE database and related tools and resources in 2019: improving support for quantification data. *Nucleic Acids Res* 47: D442 – D450

Porritt RA, Hertzog PJ (2015) Dynamic control of type I IFN signalling by an integrated network of negative regulators. *Trends Immunol* 36: 150 – 160

Rahman S, Sowa ME, Ottinger M, Smith JA, Shi Y, Harper JW, Howley PM (2011) The Brd4 extraterminal domain confers transcription activation independent of pTEFb by recruiting multiple proteins, including NSD3. *Mol Cell Biol* 31: 2641 – 2652

Rajendran P, Johnson G, Li Li, Chen Y-S, Dashwood M, Nguyen N, Ulusan A, Ertem F, Zhang M, Li J *et al* (2019) Acetylation of CCAR2 establishes a BET/BRD9 acetyl switch in response to combined deacetylase and bromodomain inhibition. *Can Res* 79: 918 – 927

Remillard D, Buckley DL, Paulk J, Brien GL, Sonnett M, Seo H-S, Dastjerdi S, Wühr M, Dhe-Paganon S, Armstrong SA *et al* (2017) Degradation of the BAF complex factor BRD9 by heterobifunctional ligands. *Angew Chem* 56: 5738 – 5743

Rice GI, Park S, Gavazzi F, Adang LA, Ayuk LA, Van Eyck L, Seabra L, Barrea C, Battini R, Belot A *et al* (2020) Genetic and phenotypic spectrum associated with IFIH1 gain-of-function. *Hum Mutat* 41: 837 – 849

Robinson MD, McCarthy DJ, Smyth GK (2010) edgeR: a Bioconductor package for differential expression analysis of digital gene expression data. *Bioinformatics* 26: 139 – 140

Rodero MP, Crow YJ (2016) Type I interferon-mediated monogenic autoinflammation: the type I interferonopathies, a conceptual overview. *J Exp Med* 213: 2527 – 2538

Rodero MP, Tesser A, Bartok E, Rice GI, Della Mina E, Depp M, Beitz B, Bondet V, Cagnard N, Duffy D *et al* (2017) Type I interferon-mediated autoinflammation due to DNase II deficiency. *Nat Commun* 8: 2176

Sakamoto S, Potla R, Larner AC (2004) Histone deacetylase activity is required to recruit RNA polymerase II to the promoters of selected interferon-stimulated early response genes. *J Biol Chem* 279: 40362 – 40367

Sanchez GAM, Reinhardt A, Ramsey S, Wittkowski H, Hashkes PJ, Berkun Y, Schalm S, Murias S, Dare JA, Brown D *et al* (2018) JAK1/2 inhibition with baricitinib in the treatment of autoinflammatory interferonopathies. *J Clin Invest* 128: 3041 – 3052

Sanjana NE, Shalem O, Zhang F (2014) Improved vectors and genome-wide libraries for CRISPR screening. *Nat Methods* 11: 783 – 784

Shaw AE, Hughes J, Gu Q, Behdenna A, Singer JB, Dennis T, Orton RJ, Varela M, Gifford RJ, Wilson SJ *et al* (2017) Fundamental properties of the mammalian innate immune system revealed by multispecies comparison of type I interferon responses. *PLoS Biol* 15: e2004086

Spahn PN, Bath T, Weiss RJ, Kim J, Esko JD, Lewis NE, Harismendy O (2017) PinAPL-Py: a comprehensive web-application for the analysis of CRISPR/Cas9 screens. *Sci Rep* 7: 15854

Spieler EE, Moritz E, Stertz S, Hale BG (2020) Application of a biologically contained reporter system to study gain-of-function H5N1 influenza A viruses with pandemic potential. *mSphere* 5: e00423-20

Stertz S, Hale BG (2021) Interferon system deficiencies exacerbating severe pandemic virus infections. *Trends Microbiol* https://doi.org/10.1016/j.tim.2021.03.001

Stewart CE, Randall RE, Adamson CS (2014) Inhibitors of the interferon response enhance virus replication *in vitro*. *PLoS One* 9: e112014

Teo G, Liu G, Zhang J, Nesvizhskii AI, Gingras AC, Choi H (2014) SAINTexpress: improvements and additional features in significance analysis of INTeractome software. *J Proteomics* 100: 37 – 43

Vangamudi B, Paul TA, Shah PK, Kost-Alimova M, Nottebaum L, Shi Xi, Zhan Y, Leo E, Mahadeshwar HS, Protopopov A *et al* (2015) The SMARCA2/4 ATPase domain surpasses the bromodomain as a drug target in SWI/SNF-mutant cancers: insights from cDNA rescue and PFI-3 inhibitor studies. *Can Res* 75: 3865 – 3878

Wang X, Wang Su, Troisi EC, Howard TP, Haswell JR, Wolf BK, Hawk WH, Ramos P, Oberlick EM, Tzvetkov EP *et al* (2019) BRD9 defines a SWI/SNF sub-complex and constitutes a specific vulnerability in malignant rhabdoid tumors. *Nat Commun* 10: 1881

Wei Z, Yoshihara E, He N, Hah N, Fan W, Pinto AFM, Huddy T, Wang Y, Ross B, Estepa G *et al* (2018) Vitamin D switches BAF complexes to protect β cells. *Cell* 173: 1135 – 1149.e15

Yan Z, Cui K, Murray DM, Ling C, Xue Y, Gerstein A, Parsons R, Zhao K, Wang W (2005) PBAF chromatin-remodeling complex requires a novel specificity subunit, BAF200, to regulate expression of selective interferon-responsive genes. *Genes Dev* 19: 1662 – 1667

Zhang Q, Bastard P, Liu Z, Le Pen J, Moncada-Velez M, Chen J, Ogishi M, Sabli IKD, Hodeib S, Korol C *et al* (2020) Inborn errors of type I IFN immunity in patients with life-threatening COVID-19. *Science* 370: eabd4570

Zhang X, Bogunovic D, Payelle-Brogard B, Francois-Newton V, Speer SD, Yuan C, Volpi S, Li Z, Sanal O, Mansouri D *et al* (2015) Human intracellular ISG15 prevents interferon-alpha/beta over-amplification and auto-inflammation. *Nature* 517: 89 – 93

Zhou Q, Huang J, Zhang C, Zhao F, Kim W, Tu X, Zhang Y, Nowsheen S, Zhu Q, Deng M *et al* (2020) The bromodomain containing protein BRD-9 orchestrates RAD51-RAD54 complex formation and regulates homologous recombination-mediated repair. *Nat Commun* 11: 2639